# Analytical probabilistic modeling of RBE-weighted dose for ion therapy

**HP Wieser[1,2], P Hennig[3], N Wahl[1,2], M Bangert[1,2]**

[1]Department of Medical Physics in Radiation Oncology,
German Cancer Research Center - DKFZ,
Im NeuenheimerFeld 280, D-69120 Heidelberg, Germany
[2] Heidelberg Institute for Radiation Oncology - HIRO,
Im Neuenheimer Feld 280, D-69120, Germany
[3] Max Planck Institute for Intelligent Systems
Spemannstraße 34, 72076 Tübingen, Germany

E-mail: `h.wieser@dkfz.de`

September 2017

**Abstract.** Particle therapy is especially prone to uncertainties. This issue is usually being addressed with uncertainty quantification and minimization techniques based on scenario sampling. For proton therapy, however, it was recently shown that it is also possible to use closed-form computations based on Analytical Probabilistic Modeling (APM) for this purpose. The APM yields unique features compared to sampling-based approaches motivating further research in this context.

This paper demonstrates the application of APM for intensity-modulated carbon ion therapy to quantify the influence of setup and range uncertainties on the RBE-weighted dose. In particular, we derive analytical forms for the nonlinear computations of the expectation value and variance of the RBE-weighted dose by propagating linearly correlated Gaussian input uncertainties through a pencil beam dose calculation algorithm. Both, exact and approximation formulas are presented for the expectation value and variance of the RBE-weighted dose and subsequently studied in-depth for a one-dimensional carbon ion spread-out Bragg peak. With $V$ and $B$ being the number of voxels and pencil beams, respectively, the proposed approximations induce only a marginal loss of accuracy while lowering the computational complexity from order $\mathcal{O}(V \times B^2)$ to $\mathcal{O}(V \times B)$ for the expectation value and from $\mathcal{O}(V \times B^4)$ to $\mathcal{O}(V \times B^2)$ for the variance of the RBE-weighted dose. Moreover, we evaluated the approximated calculation of the expectation value and standard deviation of the RBE-weighted dose in combination with a probabilistic effect-based optimization on three patient cases considering carbon ions as radiation modality against sampled references. The resulting global $\gamma$-pass rates [2 mm,2 %] are $> 99.15\,\%$ for the expectation value and $> 94.95\,\%$ for the standard deviation of RBE-weighted dose, respectively. We applied the derived analytical model to carbon ion treatment planning, although the concept is in general applicable to other ion species considering a variable RBE.

*Keywords*: probabilistic treatment planning, biological effect, particle therapy, treatment planning, carbon ion

## 1. Introduction

Treatment planning for charged particle therapy requires an accurate simulation of the dose distribution within the patient's body before delivery. In reality, various sources of uncertainty along the treatment planning work-flow e.g. imaging, dose calculation, or irradiation itself may impair the validity of the simulated dose distributions. Range and setup uncertainties are considered to be among the most influential sources of physical uncertainty (Lomax 2008a, Lomax 2008b, Paganetti 2012). Their dosimetric impact can be quantified using worst case estimates (Lowe et al. 2016, Albertini et al. 2011, Liu et al. 2013) dose blurring methods (Baum et al. 2004), dose warping techniques (Park et al. 2012), sampling meta models based on Gaussian processes (Sobotta et al. 2012), and polynomial chaos expansion (Perkó et al. 2016).

The afore mentioned uncertainties are compensated during treatment planning in current clinical practice by the design of an adequate margin, which extends the clinical target volume (CTV) to a planning target volume (PTV). This approach is either restricted to non-problematic cases where anatomical variations do not imply strong modifications of radiological depths or combined with single field uniform dose (SFUD) optimization (Lomax 2008c). Robust optimization techniques such as worst case (Pflugfelder et al. 2008, Fredriksson et al. 2011, Chen et al. 2012, Liu et al. 2012) or probabilistic optimization (Unkelbach et al. 2007, Unkelbach et al. 2009) are designed to supersede safety margins. While there are first commercial implementations available for proton therapy, there are no commercial implementations available for carbon ion therapy.

In contrast to protons, studies in robust treatment planning for heavier charged particles, such as carbon ions, are very limited. As carbon ion dose distributions exhibit steeper lateral and longitudinal dose gradients - in particular in the high dose domain directly around the target - robustness analysis and robust optimization may arguably be especially important for this modality (Suit et al. 2010). Meaningful consideration requires nonlinear modeling of the relative biological effectiveness (RBE) of carbon ions yielding a more complex treatment planning process than for protons (Jäkel et al. 2001). Steitz et.al. (2016) studied the dosimetric impact of interfactional motion on pancreatic cancer applying worst case, single-field-uniform-dose and margin-based optimization concluding that robust optimization is a valuable tool to improve the trade-off between robust target coverage and organ at risk sparing. Sakama et.al. (2016) estimated the variance of biological effective dose considering fractionation effects by using a fast dose wrapping technique based on the water equivalent path length.

At their core, all previously referenced methods rely on sampling, i.e., the simulation of a discrete set of treatment scenarios. Inevitably, this results in a trade-off between accuracy of uncertainty propagation and computational cost which is negatively affected by an increasing number of uncertain input parameters and complex correlations of the uncertainties, especially with regard to fractionation.

For intensity-modulated proton therapy, it is possible to bypass the need for sampling through the use of analytical probabilistic modeling (APM) that enables closed-form calculation of the expectation value and standard deviation of the RBE-weighted dose considering a constant RBE of 1.1 (Bangert et al. 2013). APM facilitates the incorporation of arbitrary correlation models including fractionation effects of range and setup errors at an improved accuracy to efficiency trade-off compared to conventional sampling approaches (Wahl et al. 2017). In further consequence, highly

efficient probabilistic optimization is possible.

In this paper, we generalize APM computations of the expectation value and the variance from the linear dose calculation required for proton therapy to nonlinear RBE-weighted dose calculation for carbon ions. An accurate mathematical model depicting the complex dependence of RBE on dose requires the joint incorporation of range and setup uncertainties into physical dose and RBE at the same time. Because the underlying mathematical moment computations are computationally challenging, algebraic approximations that effectively reduce complexity are introduced. The quality of the approximations are investigated in detail for a one-dimensional spread-out Bragg peak (SOBP). In addition, we investigate APM's accuracy compared to sampling based approaches on three patient cases and perform a treatment planning study using probabilistic biological effect optimization under different fractionation assumptions.

This paper is organized as follows. Section 2 repeats the basic principle of APM and derives calculations for the nominal value, expectation value, and variance of the biological effect $\varepsilon$ and RBE-weighted dose. Next, section 3 shows the application on a one-dimensional SOBP and on three patient c ases considering different fractionation schemes. Sections 4 and 5 discuss and conclude the paper.

## 2. Material and Methods

At the same physical dose, carbons ions induce a lower cell survival rate than protons mainly due to differences in the microscopic energy deposition pattern. Hence, clinical carbon ion treatment planning is based on the RBE-weighted dose with the RBE being a patient-specific nonlinear three-dimensional quantity depending, among other things, on the linear energy transfer (LET), dose level, biological endpoint, and tissue type. The RBE is defined as the ratio between iso-effective physical doses of a reference radiation $d_x$ and of particles $d_p$. In the framework of the linear quadratic (LQ) model (Kellerer & Rossi 1978), the RBE-weighted dose is given by

$$RBE \times d_p = \sqrt{\frac{\alpha_p d_p + \beta_p d_p^2}{\beta_x} + \left(\frac{\alpha_x}{2\beta_x}\right)^2} - \frac{\alpha_x}{2\beta_x} \tag{1}$$

with the parameters $\alpha_x$, $\beta_x$ ($\alpha_p$, $\beta_p$) describing the radio-sensitivity of photons (particles). The computation of the RBE-weighted dose involves an intermediate quantity, i.e., the biological effect

$$\varepsilon_p = \alpha_p d_p + \beta_p d_p^2 \tag{2}$$

which can be used as an alternative for treatment planning (Wilkens & Oelfke 2006). Via the LQ model, $\varepsilon_p$ is linked to cell survival $S$

$$S = e^{-\varepsilon_p} = e^{-\alpha_p d_p - \beta_p d_p^2}. \tag{3}$$

For algebraic convenience, we focus on the biological effect $\varepsilon$ to build an analytical probabilistic model for uncertainty propagation and not on the RBE-weighted dose. An explanation for this approach will be given at a later point where it is shown that the square root dependence in Equation 1 can be accounted for with a post processing step (see section 2.6) to ultimately obtain the desired mean and variance of the RBE-weighted-dose.

The biological effect $\boldsymbol{\varepsilon}(X)$ is considered to be a function of uncertain input parameters $X$ that follow a probability density $p(X)$. Consequently, the $n$-th raw

moment of the induced probability distribution over the biological effect $\varepsilon$ can be calculated/approximated by

$$\mathbb{E}[\boldsymbol{\varepsilon}(X)^n] = \int dX\, p(X)\boldsymbol{\varepsilon}(X)^n \approx \int dX\, \mathcal{N}(X, \bar{X}, \Sigma_X)\, \hat{\boldsymbol{\varepsilon}}(X)^n. \tag{4}$$

Equation 4 shows the basic concept of APM. Using a multivariate normal distribution $\mathcal{N}(X, \bar{X}, \Sigma_X)$ to describe the probability distribution over uncertain input parameters $p(X)$ and using a functional approximation $\hat{\boldsymbol{\varepsilon}}$ instead of the full form $\boldsymbol{\varepsilon}$, we aim at solving the integral equation in closed form. The main challenge is therefore to identify a functional approximation $\hat{\boldsymbol{\varepsilon}}$ that allows for high approximation quality and minimal computational cost at the same time.

In the following, we are going to introduce step by step the functional approximation $\hat{\boldsymbol{\varepsilon}}$ (section 2.1), the uncertainty model (section 2.2), the solution of Equation 4 to compute expectation value and variance of $\boldsymbol{\varepsilon}$ (sections 2.3 and 2.4). Finally, section 2.7 outlines the validation. In the following $i$,$l$ refer to voxel indices, $j$, $m$, $o$ refer to pencil beam indices, $V$ denotes the number of dose voxels and $B$ depicts the number of pencil beams.

### *2.1. Nominal biological effect calculation*

Throughout this work, we focus on carbon ions and obtain their tissue response ($\alpha(T,E)$, $\beta(T,E)$) from the tissue response to x-rays using the local effect model IV (LEM IV) (Scholz & Kraft 1996, Elsässer et al. 2010). Given the particle fluence $\Phi(z,T,E)$, the stopping power $SP(T,E)$, the particle type $T$, the energy $E$ and the radiological depth $z$, we follow Zaider & Rossi (1980) to obtain depth-depended dose-averaged LQ model parameter for each initial beam energy:

$$\alpha^c(z) = \frac{\sum_T \int_0^\infty \alpha(T,E)\, \Phi(z,T,E)\, SP(T,E)\, dE}{\sum_T \int_0^\infty \Phi(z,T,E)\, SP(T,E)\, dE} \tag{5}$$

A similar expression can be derived for $\sqrt{\beta^c(z)}$, but is not shown here. We decided to use LEM as it is also used for clinical treatment planning in European carbon ion therapy centers. Photon reference radio-sensitivity parameters of $\alpha_x = 0.1\,\mathrm{Gy}^{-1}$ and $\beta_x = 0.05\,\mathrm{Gy}^{-2}$ were used as LEM input, but our considerations are neither restricted to these tissue-specific values nor on LEM IV. To assess biological effects for an ensemble of particles, we follow Krämer & Scholz (2006) which limits our considerations to doses $\leq$10 Gy (RBE).

For treatment planning we use 121 tabulated carbon ion depth dose profiles, spaced from $115.23\,\mathrm{MeV\,u}^{-1}$ to $398.84\,\mathrm{MeV\,u}^{-1}$. Each integrated physical dose profile is scored as a function of depth in water and complemented by dose-averaged $\boldsymbol{\alpha}^c$ - and $\boldsymbol{\beta}^c$ profiles considering the particle spectra.

Lateral dose profiles of the carbon pencil beam are parameterized as function of depth by a single radially symmetric Gaussian. The total width of the carbon ion beam at radiological depth $z$ is determined by the initial beam width and the beam broadening caused by multiple Coloumb scattering $\lambda^2 = \sigma_{Ini}^2 + \sigma_{MC}^2(z)$. By this means, depth dependent characteristics of each of the 121 pencil beams are described by four vectors ($d(z)$, $\alpha^c(z)$, $\sqrt{\beta^c(z)}$ and $\sigma_{MC}^2(z)$) and are part of the base data used for treatment planning.

The implemented dose calculation in water is based on the pencil beam algorithm presented in Schaffner et.al. (1999) and includes a full volumetric ray tracing (Siggel et al. 2012). A detailed description of the underlying carbon dose calculation engine and a comparison to a validated treatment planning system can be found elsewhere (Wieser et al. 2017).

To account for the synergistic effects in a mixed radiation field created by ions of different energies, the calculation of the total biological effect $\varepsilon_i$ at voxel $i$ requires the calculation of dose-averaged radio-sensitivity parameters $\alpha_i^c$ and $\sqrt{\beta_i^c}$ taking into account contributions from different spots (Zaider & Rossi 1980). Let $w_j$ be the fluence weight of pencil beam $j$ and $D_{ij}$ ( $\alpha_{ij}^c/\sqrt{\beta_{ij}^c}$) the dose (LQ model parameter) contribution of pencil beam $j$ to voxel $i$. The nominal biological effect $\varepsilon_i$ is then given by Wilkens & Oelfke (2006):

$$\varepsilon_i(\boldsymbol{w}) = \alpha_i^c(\boldsymbol{w})d_i(\boldsymbol{w}) + \beta_i^c(\boldsymbol{w})d_i^2(\boldsymbol{w}) = \sum_{j=1}^{B} w_j \alpha_{ij}^c D_{ij} + \left(\sum_{j=1}^{B} w_j \sqrt{\beta}_{ij}^c D_{ij}\right)^2 \tag{6}$$

To reduce the number of computations for the calculation of the biological effect in the context of APM, physical $d(z)$ and biological beam properties $\alpha^c(z)$, $\sqrt{\beta^c}(z)$ were combined for each initial energy by multiplying the integrated depth dose profile with each of the two dose-averaged radio-sensitivity parameters of the LQ model upfront. The $\circ$ operator represents in the following the element-wise multiplication (Hadamard product) of two vectors $\boldsymbol{u}$ and $\boldsymbol{v}$, i.e, for element $x$ of the resulting vector we have $(u \circ v)_x = u_x \cdot v_x$. The resulting $\boldsymbol{\alpha^c} \circ \boldsymbol{d}$ and $\boldsymbol{\sqrt{\beta^c}} \circ \boldsymbol{d}$ profiles enable a direct derivation of the biological effect for each individual pencil beam. The elementwise multiplication $\circ$ can be understood as modelling a perfect correlation between the physical dose and its biological beam properties. A change in range, e.g. due to range uncertainties, consistently changes the corresponding depth-dependent dose-averaged $\alpha^c(z)$ and $\sqrt{\beta^c}(z)$ profiles and further the RBE-weighted dose. This assumption is inspired by Equation 6 and requires then only three ($\boldsymbol{\alpha^c} \circ \boldsymbol{d}$, $\boldsymbol{\sqrt{\beta^c}} \circ \boldsymbol{d}$ and $\boldsymbol{\sigma^2_{MC}}$) instead of four depth-dependent components to describe the characteristics of a carbon ion pencil beam.

In agreement with the conventional pencil beam model, we assume a factorization into two lateral dose components $L_{ij}^x$, $L_{ij}^y$ and one depth dose component, $Z_{ij}^{\alpha}$ and $Z_{ij}^{\sqrt{\beta}}$, respectively. Thus, the biological effect can be reformulated as

$$\varepsilon_i = \sum_{j=1}^{B} w_j L_{ij}^x L_{ij}^y Z_{ij}^{\alpha} + \left(\sum_{j=1}^{B} w_j L_{ij}^x L_{ij}^y Z_{ij}^{\sqrt{\beta}}\right)^2 . \tag{7}$$

Similar to Wilkens & Oelfke (2006) we are assuming laterally constant $\alpha^c$ and $\beta^c$, which implies they only influence the depth dependent components in Equation 6 and 7. In analogy to the physical depth dose for protons (Bangert et al. 2013), we represent depth dependent $\boldsymbol{\alpha^c} \circ \boldsymbol{d}$ and $\boldsymbol{\sqrt{\beta^c}} \circ \boldsymbol{d}$ profiles by a weighted superposition of thirteen Gaussian components. Compared to Bangert et.al (2013) we increased the number of Gaussian components by three due to the sharper peak and the additional fragmentation tail that needs to be modeled. Herewith, we switch to a representation of the tabulated base data, that allows now analytical integration. Least-squares fits for 121 initial beam energies were carried out as an off-line pre-computation (i.e. they yield tabulated coefficients that do not have to be reproduced at runtime). Thus, each pair of curves is described according to Equation 8 with a set of weights $\omega_{jk}^{\alpha}$ $\omega_{jk}^{\beta}$,

means $\mu_{jk}^{\alpha}$, $\mu_{jk}^{\beta}$ and widths $\delta_{jk}^{\alpha}$, $\delta_{jk}^{\beta}$. It is noteworthy, that each set of photon reference radio-sensitivity parameters requires a new fit.

Given the radiological depth $z_{ij}$ of voxel $i$ irradiated by pencil beam $j$, $Z_{ij}^{\alpha}$ and $Z_{ij}^{\surd\beta}$ can be obtained via:

$$Z_{ij}^{\alpha} = \sum_{k=1}^{13} \frac{\omega_{jk}^{\alpha}}{\sqrt{2\pi {\delta_{jk}^{\alpha}}^2}} e^{\frac{\left(z_{ij}-\mu_{jk}^{\alpha}\right)^2}{2{\delta_{jk}^{\alpha}}^2}} \quad \text{and} \quad Z_{ij}^{\surd\beta} = \sum_{k=1}^{13} \frac{\omega_{jk}^{\beta}}{\sqrt{2\pi {\delta_{jk}^{\beta}}^2}} e^{\frac{\left(z_{ij}-\mu_{jk}^{\beta}\right)^2}{2{\delta_{jk}^{\beta}}^2}} \tag{8}$$

Figure 1a depicts physical and biological beam properties of a single energy carbon ion beam of 277 MeV u$^{-1}$ and Figure 1b illustrates the achieved fit for the corresponding $\boldsymbol{\alpha^c \circ d}$ profile. The mean relative difference to the reference data amounts to 0.25 % for $\boldsymbol{\alpha^c \circ d}$ profiles and 0.06 % for $\boldsymbol{\surd\beta^c \circ d}$ profiles.

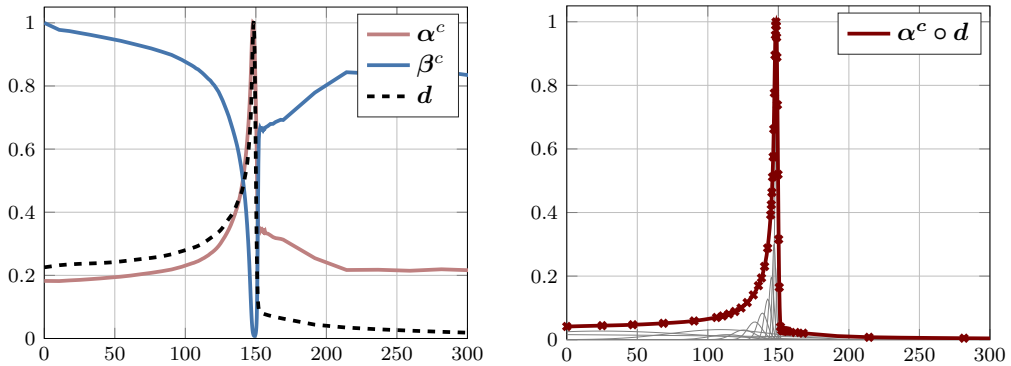


(a) z [mm] (b) z [mm]

Figure 1: (a) normalized integrated carbon ion depth dose profile of a 227 MeV u$^{-1}$ beam (dashed black line) and corresponding dose-averaged $\boldsymbol{\alpha}^c$ (solid red) and $\boldsymbol{\beta}^c$ (solid blue) curves of the LQ model predicted by LEMIV using $\alpha_x = 0.1\,\mathrm{Gy}^{-1}$ and $\beta_x$ =0.05 Gy$^{-2}$. (b) $\boldsymbol{\alpha^c \circ d}$ - profile (red solid line) of a 277 MeV carbon ion beam represented by a weighted superposition of thirteen Gaussian components (solid grey) . Crosses indicate reference values.

Next, let $x_{ij}/y_{ij}$ be the lateral distances of voxel $i$ to the central ray of pencil beam $j$, $\lambda_{ij}^2$ be the beam width of voxel $i$ and pencil beam $j$ at radiological depth $z_{ij}$, $\mathcal{N}(x;\mu,\lambda)$ be a Gaussian distribution with mean $\mu$ and standard deviation $\lambda$ evaluated at $x$, then Equation 7 can be rewritten to only rely on Gaussian components:

$$\varepsilon_i = \sum_{j=1}^{B} w_j\, \mathcal{N}(x_{ij};\mu_j^x,\lambda_{ij})\,\mathcal{N}(y_{ij};\mu_j^y,\lambda_{ij}) \sum_{k=1}^{13} \omega_{jk}^{\alpha}\, \mathcal{N}(z_{ij};\mu_{jk}^{\alpha},\delta_{jk}^{\alpha}) + \left( \sum_{j=1}^{B} w_j\, \mathcal{N}(x_{ij};\mu_j^x,\lambda_{ij})\,\mathcal{N}(y_{ij};\mu_j^y,\lambda_{ij}) \sum_{k=1}^{13} \omega_{jk}^{\beta}\, \mathcal{N}(z_{ij};\mu_{jk}^{\beta},\delta_{jk}^{\beta}) \right)^2 \tag{9}$$

Consequently, Equation 9 renders the calculation of the expectation value and variance of the biological effect according to Equation 4 analytically tractable.

### *2.2. Uncertainty model*

Setup and range errors are considered individually for each pencil beam by modelling offsets $\boldsymbol{\Delta}^x \in \mathbb{R}^B$, $\boldsymbol{\Delta}^y \in \mathbb{R}^B$, and $\boldsymbol{\Delta}^z \in \mathbb{R}^B$ in the Gaussian components underlying the biological effect calculation

$$\varepsilon_i = \sum_{j=1}^{B} w_j \, \mathcal{N}(x_{ij} + \Delta_j^x; \mu_j^x, \lambda_{ij}) \, \mathcal{N}(y_{ij} + \Delta_j^y; \mu_j^y, \lambda_{ij}) \sum_{k=1}^{13} \omega_{jk}^{\alpha} \, \mathcal{N}(z_{ij} + \Delta_j^z; \mu_{jk}^{\alpha}, \delta_{jk}^{\alpha}) + \left( \sum_{j=1}^{B} w_j \, \mathcal{N}(x_{ij} + \Delta_j^x; \mu_j^x, \lambda_{ij}) \, \mathcal{N}(y_{ij} + \Delta_j^y; \mu_j^y, \lambda_{ij}) \sum_{k=1}^{13} \omega_{jk}^{\beta} \, \mathcal{N}(z_{ij} + \Delta_j^z; \mu_{jk}^{\beta}, \delta_{jk}^{\beta}) \right)^2 \quad (10)$$

$\boldsymbol{\Delta}^x$, $\boldsymbol{\Delta}^y$, and $\boldsymbol{\Delta}^z$ stem from a joint probability distribution $p(\boldsymbol{\Delta}^x, \boldsymbol{\Delta}^y, \boldsymbol{\Delta}^z)$which factorizes into a product of three multivariate normal distributions with zero mean

$$p(\boldsymbol{\Delta}^x, \boldsymbol{\Delta}^y, \boldsymbol{\Delta}^z) = \mathcal{N}(\boldsymbol{\Delta}^x; 0, \Sigma^x) \, \mathcal{N}(\boldsymbol{\Delta}^y; 0, \Sigma^y) \, \mathcal{N}(\boldsymbol{\Delta}^z; 0, \Sigma^z). \quad (11)$$

The covariance matrices $\Sigma^x$, $\Sigma^y$, $\Sigma^z$ allow to explicitly model the magnitude of uncertainty of arbitrary pairwise pencil beam correlations and have to be defined upfront according to the uncertainty assumptions. Here, we assume setup errors to be perfectly correlated for pencil beams belonging to the same beam direction, whereas pencil beam pairs stemming from different beam directions are uncorrelated. Range uncertainties are perfectly correlated for pencil beams impinging on the same lateral position as carbon ions and fragments penetrate the same tissue (Unkelbach et al. 2009).

The APM formalism allows to consider fractionation effects by exploiting a correlation model on the interplay of systematic and random errors over multiple treatment fractions. Thereby, the computation complexity is constant for an increasing number of fractions (Bangert et al. 2013). Throughout this article, setup errors are assumed to be comprised of a 1 mm systematic- and a 2 mm random-error. In addition, range errors are described by a relative systematic error component of 3.5 % and a random error of 1 mm.

The probability density $p(\boldsymbol{\Delta}^x, \boldsymbol{\Delta}^y, \boldsymbol{\Delta}^z)$ induces uncertainty over $\varepsilon_i$ that can be described with a probability distribution $p(\varepsilon_i)$ which is of non-Gaussian form. The functional approximation of the biological effect calculation along with the uncertainty assumptions made in this section enable the calculation of statistical moments of the biological effect $\boldsymbol{\varepsilon}$ in closed-form. Hence, analytical expressions for the expectation value $\mathbb{E}[\boldsymbol{\varepsilon}]$ and the covariance matrix $\mathbb{E}[\boldsymbol{\varepsilon}\boldsymbol{\varepsilon}^T] - \mathbb{E}[\boldsymbol{\varepsilon}]\mathbb{E}[\boldsymbol{\varepsilon}]^T$ can be derived. Here $\mathbb{E}[\cdot]$ denotes the expectation operator. In general, it is possible to obtain also analytical expression for higher order moments (e.g. skewness, kurtosis) to better describe the unknown shape of the probability density of $p(\varepsilon_i)$, but this is beyond the scope of this paper.

### *2.3. Expected biological effect*

To increase readability for the following deviations, Appendix A depicts a lookup table explaining the notation employed in this chapter. To calculate the expectation value, i.e., the first raw moment of the biological effect in closed-form considering setup and range uncertainties, Equation 12 needs to be solved:

$$\mathbb{E}[\varepsilon_i] = \int d\boldsymbol{\Delta}^x d\boldsymbol{\Delta}^y d\boldsymbol{\Delta}^z \, p(\boldsymbol{\Delta}^x) p(\boldsymbol{\Delta}^y) p(\boldsymbol{\Delta}^z) \varepsilon_i(\boldsymbol{\Delta}^x, \boldsymbol{\Delta}^y, \boldsymbol{\Delta}^z). \quad (12)$$

The computations require standard Gaussian algebra as exercised in Appendix B or in Equations 13-18 in (Bangert et al. 2013) yielding the form

$$\mathbb{E}[\varepsilon_i] = \sum_j^B w_j \mathcal{L}_{ij}^x \mathcal{L}_{ij}^y \mathcal{Z}_{ij}^\alpha + \sum_{jm}^B w_j w_m \Upsilon_{ijim}^x \Upsilon_{ijim}^y \Xi_{ijim}^{\sqrt{\beta}}. \tag{13}$$

Due to the quadratic term in the biological effect, the calculation of its expectation value requires the $4^{th}$ order terms $\Upsilon_{ijim}^{x/y}$ and $\Xi_{ijim}^{\sqrt{\beta}}$, representing the second raw moment of $L_{ij}^{x/y}$, $Z_{ij}^{\sqrt{\beta}}$. These $4^{th}$ order terms model the influence of pencil beam combinations $jm$ of the quadratic term on the expected biological effect $\mathbb{E}[\varepsilon_i]$ and emerge by integrating the biological effect $\varepsilon_i$ against Gaussian densities as illustrated in Equation 12. However, for fraction doses of individual pencil beams, we have $\boldsymbol{\alpha^c} \circ \boldsymbol{d} >> (\sqrt{\boldsymbol{\beta^c}} \circ \boldsymbol{d})^2$ and consequently the biological effect is mainly determined by the linear part (first additive term in Equation 13) of the biological effect (Kamp et al. 2014). Therefore, we suggest that covariance elements (i.e., $j \neq m$) in $\Upsilon_{ijim}^{x/y}$ and $\Xi_{ijim}^{\sqrt{\beta}}$ can be neglected for a first approximation in the calculation of $\mathbb{E}[\varepsilon_i]$. This reduces the number of computations and can be interpreted as neglecting the influence of the interdependence of $L_{ij/im}^{x/y}$, $Z_{ij/im}^{\sqrt{\beta}}$ on the quadratic term of the expectation value of the biological effect $\mathbb{E}[\varepsilon_i]$. As a result, the second raw moments $\Upsilon_{ijim}^{x/y}$, and $\Xi_{ijim}^{\sqrt{\beta}}$ are approximated by squaring the first raw moments $\mathcal{L}_{ij}^{x/y}$, $\mathcal{Z}_{ij}^{\sqrt{\beta}}$, which corresponds to only considering the trace ($j = m$) of $\Upsilon_{ijim}^{x/y}$ and $\Xi_{ijim}^{\sqrt{\beta}}$. Through this formulation, the full analytical calculation of $\mathbb{E}[\varepsilon_i]$ in Equation 13 can be approximated with $\hat{\mathbb{E}}[\varepsilon_i]$ in Equation 14 and has then the same computational complexity as the calculation of the nominal biological effect according to Equation 7.

$$\hat{\mathbb{E}}[\varepsilon_i] = \sum_j^B w_j \mathcal{L}_{ij}^x \mathcal{L}_{ij}^y \mathcal{Z}_{ij}^\alpha + \left( \sum_j^B w_j \mathcal{L}_{ij}^x \mathcal{L}_{ij}^y \mathcal{Z}_{ij}^{\sqrt{\beta}} \right)^2 = \sum_j^B w_j \mathcal{A}_{ij} + \left( \sum_j^B w_j \mathcal{B}_{ij} \right)^2 \tag{14}$$

Assessing the expectation value of the biological effect $\hat{\mathbb{E}}[\boldsymbol{\varepsilon}]$ reduces to computations of $\mathcal{L}_{ij}^{x/y}$ and $\mathcal{Z}_{ij}^{\alpha/\sqrt{\beta}}$ according to Equation B.2 and B.3, respectively. For optimization, these quantities are stored in influence matrices $\mathcal{A} = \mathbb{E}[A]$ and $\mathcal{B} = \mathbb{E}[B]$ facilitating a linear-quadratic mapping for pencil beam weights to the expected biological effect.

### *2.4. Covariance of biological effect*

The calculation of the covariance of the biological effect $\Sigma^\varepsilon$ requires the evaluation of mixed terms $\mathbb{E}[\varepsilon_i \varepsilon_l]$

$$\Sigma^\varepsilon[\varepsilon_i, \varepsilon_l] = \mathbb{E}[\varepsilon_i \varepsilon_l] \; - \; \mathbb{E}[\varepsilon_i]\, \mathbb{E}[\varepsilon_l] \tag{15}$$

Given the voxel indices $i$, $l$, the pencil beam indices $j$, $m$, $o$, $q$ and let $V$ be the

number of voxels, $B$ be the number of pencil beams, mixed terms take then the form

$$\begin{aligned}\mathbb{E}[\varepsilon_i\varepsilon_l] &= \int d\boldsymbol{\Delta}^x d\boldsymbol{\Delta}^y d\boldsymbol{\Delta}^z p(\boldsymbol{\Delta}^x)p(\boldsymbol{\Delta}^y)p(\boldsymbol{\Delta}^z)p(\boldsymbol{\Delta}^z)\varepsilon_i(\boldsymbol{\Delta}^x,\boldsymbol{\Delta}^y,\boldsymbol{\Delta}^z)\varepsilon_l(\boldsymbol{\Delta}^x,\boldsymbol{\Delta}^y,\boldsymbol{\Delta}^z) \\ &= \sum_{jm}^{B} w_j w_m \Upsilon^x_{ijlm}\Upsilon^y_{ijlm}\Xi^{\alpha}_{ijlm} + 2\sum_{jmo}^{B} w_j w_m w_o \Upsilon^x_{ijlmio}\Upsilon^y_{ijlmio}\Xi^{\alpha 2\sqrt{\beta}}_{ijlmio} + \\ &\quad \sum_{jmoq}^{B} w_j w_m w_o w_q \Upsilon^x_{ijiolmlq}\Upsilon^y_{ijiolmlq}\Xi^{\sqrt{\beta}}_{ijiolmlq} \end{aligned} \tag{16}$$

The derivation of Equation 16 and a description of the calculations of the $6^{th}$ order $\Xi^{\alpha 2\sqrt{\beta}}_{ijlmio}$ and $8^{th}$ order $\Xi^{8th\sqrt{\beta}}_{ijiolmlq}$ terms can be found in Appendix C. As we are interested in the variance of the biological effect, which is stored in the diagonal of the covariance matrix $\Sigma^{\varepsilon}[\varepsilon_i,\varepsilon_l]$, we can explicitly drop additional voxel indices $l$ and Equation 16 can be reformulated to obtain:

$$\begin{aligned}\mathbb{E}[\varepsilon_i\varepsilon_i] &= \sum_{jm}^{B} w_j w_m \Upsilon^x_{ijm}\Upsilon^y_{ijm}\Xi^{\alpha}_{ijm} + 2\sum_{jmo}^{B} w_j w_m w_o \Upsilon^x_{ijmo}\Upsilon^y_{ijmo}\Xi^{\alpha 2\sqrt{\beta}}_{ijmo} + \\ &\quad \sum_{jmoq}^{B} w_j w_m w_o w_q \Upsilon^x_{ijmoq}\Upsilon^y_{ijmoq}\Xi^{\sqrt{\beta}}_{ijmoq}. \end{aligned} \tag{17}$$

Elements of these tensors correspond then to two- (e.g. $\Upsilon^x_{ijm}$), three- (e.g. $\Upsilon^x_{ijmo}$) and four- (e.g. $\Upsilon^x_{ijmoq}$) dimensional Gaussian distributions which are the results of integration over a bivariate, trivariate and quadvariate Gaussian distribution. Components in the first additive term (e.g. $\Upsilon^x_{ijm}$) are in $\mathbb{R}^{V\times B^2}$, which would result for a typical clinical scenario with $10^6$ voxels and $2\cdot 10^4$ pencil beams in $10^6\times 2\cdot 10^4\times 2\cdot 10^4 = 4\cdot 10^{14}$ tensor elements. Components in the second additive term (e.g. $\Upsilon^x_{ijmo}$) are in $\mathbb{R}^{V\times B^3}$ and quantities in the third additive term (e.g. $\Upsilon^x_{ijmoq}$) are in order $\mathbb{R}^{V\times B^4}$. These terms represent the second, third and fourth raw moment of the lateral/depth components $L^{x/y}, Z^{\alpha}, Z^{\sqrt{\beta}}$ in voxel $i$. Calculation of these high-dimensional tensors is associated with prohibitive computational complexity in a clinical setting.

Consequently, we propose exactly the same approximation as exercised previously for the calculation of the expectation value of the biological effect and neglect all covariance terms of different pencil beams emerging from $\sqrt{\boldsymbol{\beta}^{\boldsymbol{c}}}\circ\boldsymbol{d}$ terms. As the linear term $\boldsymbol{\alpha}^{\boldsymbol{c}}\circ\boldsymbol{d}$ of the biological effect dominates compared to the squared term $(\sqrt{\boldsymbol{\beta}^{\boldsymbol{c}}}\circ\boldsymbol{d})^2$ the contribution to the biological effect in the case of fraction doses, terms that are quadratic, cubic or even quadric in $\sqrt{\boldsymbol{\beta}^{\boldsymbol{c}}}\circ\boldsymbol{d}$ only correspond to a minor correction of the overall computation. Hence, tensors like $\Xi^{\alpha 2\sqrt{\beta^c}}_{ijmo}$ and $\Xi^{8th\sqrt{\beta^c}}_{ijmoq}$ containing the $\sqrt{\boldsymbol{\beta}^{\boldsymbol{c}}}\circ\boldsymbol{d}$ dose term have decaying contributions from terms of higher order. Neglecting the covariance in terms containing $\sqrt{\boldsymbol{\beta}^{\boldsymbol{c}}}\circ\boldsymbol{d}$ then yields an approximation of the mixed term:

$$\hat{\mathbb{E}}[\varepsilon_i\varepsilon_i] = \sum_{jm}^{B} w_j w_m \Upsilon^x_{ijm}\Upsilon^y_{ijm}\Xi^\alpha_{ijm} + 2\sum_{jmo}^{B} w_j w_m w_o \Upsilon^x_{ijm}\mathcal{L}^x_{io}\,\Upsilon^y_{ijm}\mathcal{L}^y_{io}\,\mathcal{Z}^\alpha_{ij}\mathcal{Z}^{\surd\beta}_{im}\mathcal{Z}^{\surd\beta}_{io} + \sum_{jm}^{B} w_j w_m (\Upsilon^x_{ijm})^2(\Upsilon^z_{ijm})^2(\mathcal{Z}^{\surd\beta}_{ij}\mathcal{Z}^{\surd\beta}_{im})^2 = \sum_{jm}^{B} w_j w_m \hat{\mathfrak{D}}^\varepsilon_{ijm} \tag{18}$$

where $\hat{\mathfrak{D}}^\varepsilon_{ijm}$ denotes the trace of the full variance influence tensor $\hat{\mathfrak{D}}^\varepsilon_{ijlm}$. The last step of Equation 18 collapses the sum for $w_o$ in the second term to reduce the dimensionality for further considerations. Herewith, the integration over trivariate Gaussian distributions factorizes into the integration over univariate and bivariate Gaussian distributions. Analogous, the integration over quadvariate Gaussian distributions is represented by the product of two integrated bivariate Gaussian distributions. This reduces the computational complexity and storage requirements for the second raw moment of the probability distribution of the biological effect from $\mathcal{O}(V \times B^4)$ to $\mathcal{O}(V \times B^2)$. Substituting 18 in 15 yields the second central moment of the biological effect:

$$\hat{\sigma}^2[\varepsilon_i] = \hat{\Sigma}^\varepsilon[\varepsilon_i,\varepsilon_i] = \hat{\mathbb{E}}[\varepsilon_i\varepsilon_i] - \hat{\mathbb{E}}[\varepsilon_i]\,\hat{\mathbb{E}}[\varepsilon_i] = \sum_{jm}^{B} w_j w_m \mathfrak{V}^\varepsilon_{ijm} = \sum_{jm}^{B}\left(w_j w_m \hat{\mathfrak{D}}^\varepsilon_{ijm} - \left[\mathcal{A}_{ij}w_j + (\mathcal{B}_{ij}w_j)^2\right]\left[\mathcal{A}_{im}w_m + (\mathcal{B}_{im}w_m)^2\right]\right) \tag{19}$$

Besides higher storage requirements and the two to threefold increased numerical computations required for biological treatment planning in relation to treatment planning based on the physical dose, the complexity of the approximated variance calculation of the biological effect equals the complexity of the variance of the physical dose. If not stated otherwise, calculations of the expectation value and variance of the biological effect are for the remainder of this paper based on the approximations shown in Equations 14 and 18.

### *2.5. Probabilistic optimization of the biological effect*

The expectation value $\mathbb{E}[\boldsymbol{\varepsilon}]$ and the covariance $\Sigma^{\boldsymbol{\varepsilon}}$ of the biological effect together constitute a Gaussian approximation of the probability density of the biological effect.

$$p(\boldsymbol{\varepsilon}) = \mathcal{N}\left(\boldsymbol{\varepsilon}, \mathbb{E}[\boldsymbol{\varepsilon}], \Sigma^{\boldsymbol{\varepsilon}}\right) \tag{20}$$

This representation enables a probabilistic optimization using a piece-wise quadratic objective function according to Unkelbach & Oelfke (2004) and Bangert et.al. (2013). With the diagonal penalty matrix $P = diag(p_1, p_2, ..., p_N)$ and the prescribed biological effect $\boldsymbol{\varepsilon}^*$, the expected value of the piece-wise quadratic objective function is given by

$$\mathbb{E}[\mathcal{F}] = \mathrm{tr}(P\Sigma^{\boldsymbol{\varepsilon}}) + \left(\mathbb{E}[\boldsymbol{\varepsilon}] - \boldsymbol{\varepsilon}^*\right)^T P\left(\mathbb{E}[\boldsymbol{\varepsilon}] - \boldsymbol{\varepsilon}^*\right) \tag{21}$$

which can be evaluated very efficiently during optimization (Bangert et al. 2013, Wahl et al. 2017).

### *2.6. Nonlinear conversion of moments of the biological effect to moments of RBE-weighted Dose*

Clinical decision making and treatment plan evaluation in carbon ion therapy are usually based on the RBE-weighted dose. For this reason, the expectation value and variance of the biological effect are converted to expectation value and variance of RBE-weighted dose using a Taylor expansion, a commonly known error- or uncertainty propagation method. In particular, a fourth order Taylor expansion at $\mathbb{E}[\varepsilon_i]$ evaluating partial derivatives at $\varepsilon_i$ is employed to approximate the nonlinear conversion of moments of the biological effect (Anderson & Mattson 2012). The nonlinearity is brought in by the square root of a scaled version of the biological effect in Equation 1. Given $\gamma = \frac{\alpha_x}{2\beta_x}$, the propagation of moments takes then the following form:

$$\mathbb{E}[RBE \times d_i] \approx \sqrt{\beta_x^{-1}\mathbb{E}[\varepsilon_i] + \gamma^2} - \gamma - \frac{\beta_x^{-2}}{8(\beta_x^{-1}\mathbb{E}[\varepsilon_i] + \gamma^2)^{\frac{3}{2}}}\sigma[\varepsilon_i]^2 - \frac{5\beta_x^{-4}}{128(\beta_x^{-1}\mathbb{E}[\varepsilon_i] + \gamma^2)^{\frac{7}{2}}}\sigma[\varepsilon_i]^2 \tag{22}$$

$$\sigma[RBE \times d_i]^2 \approx \frac{\beta_x^{-1}}{2(\beta_x^{-1}\mathbb{E}[\varepsilon_i] + \gamma^2)^{\frac{1}{2}}}\sigma[\varepsilon_i]^2 + \frac{1}{2}\left(\frac{\beta_x^{-2}}{8(\beta_x^{-1}\mathbb{E}[\varepsilon_i] + \gamma^2)^{\frac{3}{2}}}\right)^2 \sigma[\varepsilon_i]^4 \tag{23}$$

The Taylor expansion around $\varepsilon_i$ is only locally valid meaning the approximation quality generally shrinks when the variance of the biological effect increases. Furthermore, potential deviation from the Gaussian form (e.g. skewness or bimodal distributions) that is not captured by a simple two variable model may compromise error propagation.

### *2.7. Validation*

The accuracy of the proposed analytical approximations for the expectation value and variance of the biological effect was investigated on an simplified artificial example in Section 3.1. A one-dimensional carbon ion SOBP with 150 mm range and 50 mm modulation was investigated considering 3.5 % range uncertainty. The SOBP was optimized performing an effect-based optimization according to Wilkens & Oelfke (2006). The resulting probabilistic quantities are compared against sampled references in terms of maximal deviation.

As the approximations closely match to the sampled values we demonstrate the use of APM for carbon ions in three concrete clinical settings in Section 3.2. Specifically, we evaluated the APM formalism in a treatment planning study using conventional and probabilistic optimization considering setup-, range-errors and fractionation effects. Information about uncertainty assumptions are given in section 2.2 and details about the patient cases and treatment plan parameters can be found in Table 1.

For each case, we investigated the accuracy of APM moment computations for carbon ions in comparison to random sampling for unfractionated treatment (fraction $f = 1$). The objective function applied for treatment planning features squared deviation objectives with a prescribed fraction dose of 3 Gy(RBE) for the CTV and squared overdosing objectives for the outer contour and critical structures. We perform both conventional optimization and probabilistic optimization according to Equation 21. Three-dimensional $\gamma$-pass rates according to Low et.al (1998), utilizing a distance to agreement of 2 mm and a dose difference criterion of 2 % was used for evaluation.

| | unit | intra-cranial | para-spinal | prostate |
|---|---|---|---|---|
| gantry angles | [°] | 50°, 135° | 135°, 180°, 225° | 90°, 180° |
| couch angles | [°] | 0°, 0° | 0°, 0°, 0° | 0°, 0° |
| lat. spot distance | [mm] | 3 | 4 | 5 |
| resolution | [mm$^3$] | $(1.2 \times 1.2 \times 3)$ | $(3 \times 3 \times 3)$ | $(2 \times 2 \times 3)$ |
| # pencil beam | - | 2022 | 17756 | 15669 |
| # voxels $\sigma$ | - | $0.95 \times 10^5$ | $1.2 \times 10^5$ | $0.83 \times 10^5$ |
| # fractions f | - | 1 | 5 | 20 |
| pres. fraction dose | [Gy(RBE)] | 3 | 3 | 3 |

Table 1: Information about the three different patient cases and their corresponding plan parameters. The third row lat. spot distance denotes the lateral spot spacing in the isocenter plane and # voxels $\sigma$ depicts the number of voxels for which standard deviation was calculated. The number of pencil beams and the number of voxels for $\sigma$ calculation are the dominant factors for the overall runtime.

Both the 1D SOBP as well as the patient cases are compared against sampled references. Using 5000 samples ensures the standard error of the sampled mean $\sigma[\mathbb{E}[\boldsymbol{\varepsilon}]]$ to fall below 1.4% and the expected relative error of the standard deviation $\sigma[\sigma[\boldsymbol{\varepsilon}]]$ to drop below 1% (Squires 2001).

For a proof of principle, the moment computations for carbon ions were implemented in matRad, an open-source treatment planning toolkit (Wieser et al. 2017), which is entirely written in the numerical computation environment Matlab (2016b, The MathWorks Inc).

All results presented in this manuscript are based on photon reference radio-sensitivity parameters $\alpha_x = 0.1\,\mathrm{Gy}^{-1}$ and $\beta_x = 0.05\,\mathrm{Gy}^{-2}$. We assumed a single biological system and assigned these tissue specific parameters to all patient voxles.

## 3. Results

### *3.1. Uncertainty quantification of a 1D SOBP*

The one-dimensional carbon ion spread-out Bragg peak (SOBP) is shown in Figure 2a and was computed according to Equation 9. Figure 2b considers the same SOBP, however, with 3.5 % range uncertainty.

Figure 2b compares the full analytical computation $\mathbb{E}[\boldsymbol{\varepsilon}]$ , its approximation $\hat{\mathbb{E}}[\boldsymbol{\varepsilon}]$ and sampled references of the expected biological effect. The individual terms $\mathcal{Z}^{\alpha}\boldsymbol{w}$ and $(\mathcal{Z}^{\sqrt{\beta}}\boldsymbol{w})^2$ contributing to the approximated expectation value of the biological effect $\hat{\mathbb{E}}[\boldsymbol{\varepsilon}]$ according to Equation 14 are also shown. Figure 2c explicitly visualizes the quality of the approximation for $(\mathcal{Z}^{\sqrt{\beta}}\boldsymbol{w})^2$ against the full analytical calculation $\boldsymbol{w}^T\Xi^{\sqrt{\beta}}\boldsymbol{w}$. As the maximum difference between the full analytical expected biological effect $\mathbb{E}[\boldsymbol{\varepsilon}]$ based on Equation 12 and the approximated expected biological effect $\hat{\mathbb{E}}[\boldsymbol{\varepsilon}]$ introduced in Equation 14 amounts only to 0.18%, we use the latter for further considerations. The maximum difference of the expected biological effect $\mathbb{E}[\boldsymbol{\varepsilon}]$ based on sampling (shown by green crosses in 2b) to the full analytical calculation of the biological effects using 5000 samples is 0.39 %.

Figure 3 shows the variance calculation of the biological effect as laid out in

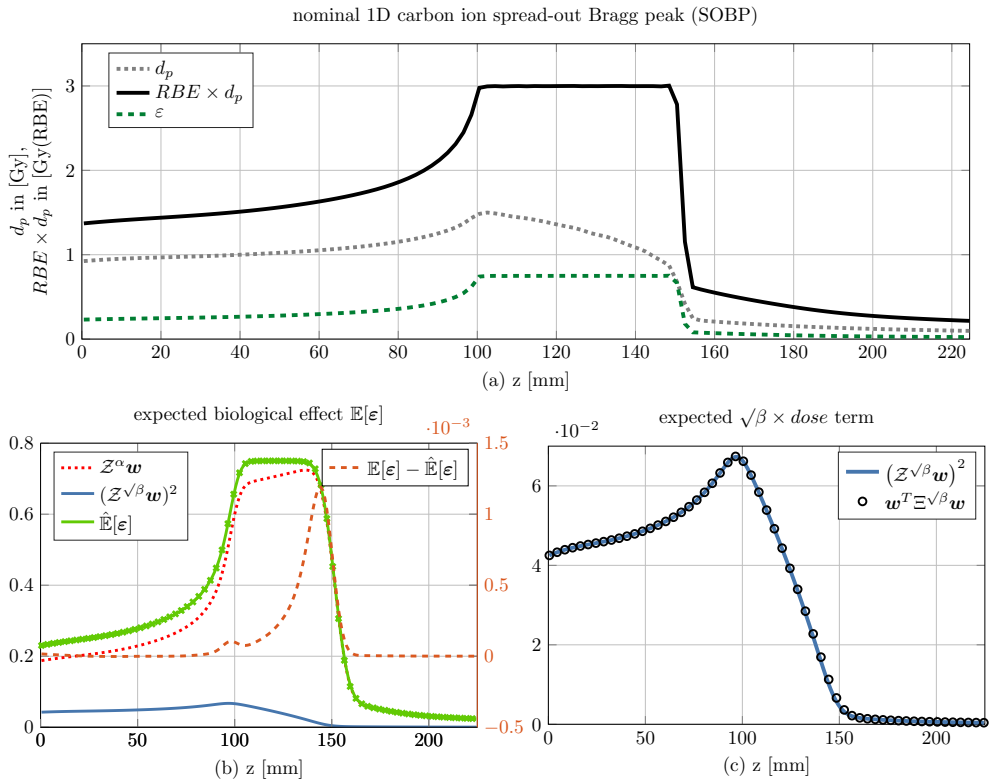


Figure 2: (a) nominal physical dose $d_p$, RBE-weighted dose ($RBE \times d_p$, and biological effect $\boldsymbol{\varepsilon}$ of a 1D carbon ion SOBP with range 150 mm and 50 mm modulation. Calculations are based on photon radio-sensitivity parameter $\alpha_x = 0.1\,\mathrm{Gy}^{-1}$ and $\beta_x = 0.05\,\mathrm{Gy}^{-2}$. Prescribed target dose is 3 Gy(RBE). (b) approximated expected biological effect $\hat{\mathbb{E}}[\boldsymbol{\varepsilon}]$ (solid green) and its components (solid blue and dotted red) considering a range uncertainty of 3.5 %. The difference between approximate and full expected biological effect calculation is shown in dashed orange (note the different scale on the right). Additionally, the expected biological effect from 5000 sampling experiments is shown by green crosses. (c) depicts the differences of the proposed approximation (solid blue line) to the full analytical calculation (black circles) of the term $(\mathcal{Z}^{\sqrt{\beta}}\boldsymbol{w})^2$. Note that the blue solid lines in Figure 2b and Figure 2c are the same.

section 2.4. Discrepancies between $\hat{\sigma}[\boldsymbol{\varepsilon}]$ and the sampled standard deviation were caused by neglecting correlations in $\sqrt{\boldsymbol{\beta}^{\boldsymbol{c}}} \circ \boldsymbol{d}$ but did not exceed 5.2 %; the root mean squared error was 0.002 [$\varepsilon$ is a dimensionless quantity]. One way to increase the accuracy of the standard deviation of the biological effect was to additionally consider covariance elements in the second additive term in Equation 17. Doing so reduced the maximum relative deviation to 2.3 % and the RMSE to 0.0016. Finally, a full analytical calculation of $\sigma[\boldsymbol{\varepsilon}]$ based on Equation 17 further lowered the maximum relative deviation to 0.9 %.

Exemplary, the histogram on the vertical axis in Figure 3 shows the actual distribution of the biological effect of a single voxel at depth $z = 150$ mm obtained by means of

sampling. As this voxel is located at the distal fall off of the SOBP, small range shifts result either in a biological effect of ∼0.75 (high-effect) or ∼0.1 (low-effect region). This behaviour is reflected by the bimodal shaped probability distribution with peaks at ∼0.75 and ∼0.1. For subsequent error propagation into RBE-weighted dose, however, we use a Gaussian probability density (solid black line on the vertical axis) as we only calculate analytically the expectation value and standard deviation of the unknown probability distribution of the biological effect.

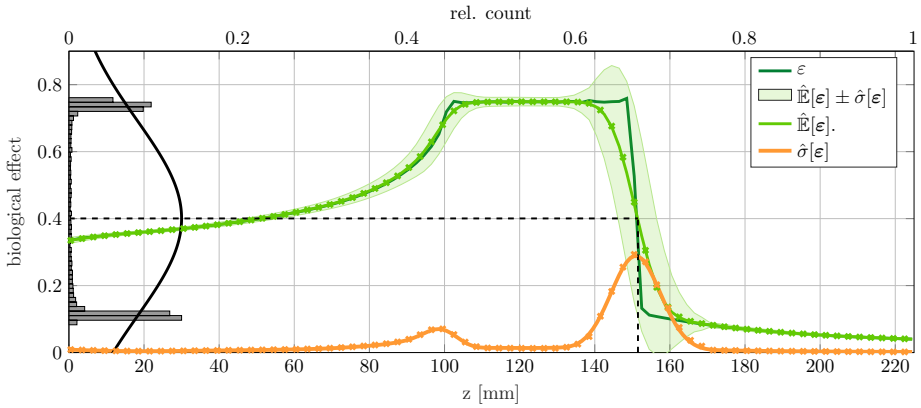


Figure 3: biological effect of a 1D C12 SOBP. The dark green solid line represents the nominal biological effect $\boldsymbol{\varepsilon}$. The bright green solid line visualizes the expected biological effect $\hat{\mathbb{E}}[\boldsymbol{\varepsilon}]$ considering 3.5% range uncertainty. The orange solid line depicts the approximated standard deviation of the biological effect $\hat{\sigma}[\boldsymbol{\varepsilon}]$. Crosses indicate sampling results ($N = 5000$). The histogram on the y axis visualizes the probability distribution of the biological effect for z = 150 mm. Gaussian approximation based on the computed expectation value and variance (solid black) does not capture the bimodal distribution of the biological effect in high variance regions.

### *3.2. Application of APM on patient cases*

Resulting $\hat{\mathbb{E}}[RBE \times d_p]$ - and $\hat{\sigma}[RBE \times d_p]$ distributions based on conventional- and probabilistic-optimization, for the transversal iso-center slices for all three patient cases are shown in Figure 4, whereas $\hat{\mathbb{E}}[RBE \times d_p]$- and $\hat{\sigma}[RBE \times d_p]$ were established according to the approximated analytical pipeline (APM) in section 2.

Similar to previous reports on probabilistic optimization with protons (Unkelbach et al. 2009) and worst case optimization with carbon ions (Steitz et al. 2016), APM creates a high dose margin around the CTV resulting in a reduced standard deviation inside the CTV while at the same time lowering the standard deviation within the organs at risk. This phenomenon is also reflected in the corresponding standard deviation volume histogram in Figure 5a. Similar results are observed for the other patient cases considering different fractionation schemes (Figures 5b and 5c).

Calculation times for a complete clinical work-flow including the calculation of the expectation value and standard deviation of the RBE-weighted dose as well as a probabilistic optimization ranged between 4 and 7 hours for individual patient cases

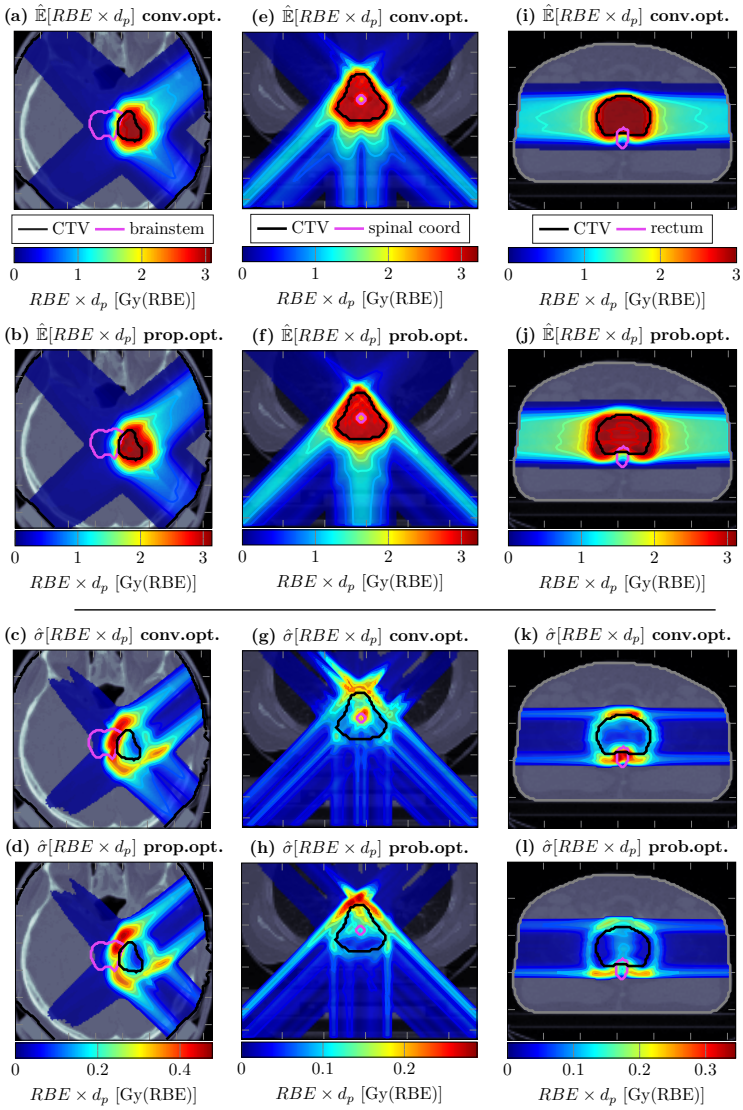


Figure 4: Transversal slices of intensity-modulated carbon ion therapy treatment plans defined in Table 1 assuming different number of fractions. The CT data is superimposed with transparent dose colorwash, solid iso-dose lines, and contours of volumes of interest. Figures 4a-4d refer to the intra-cranial case, 4e-4h to the para-spinal case and 4i-4l to the prostate case. The expectation value and standard deviation of the RBE-weighted dose based on a conventional optimization (labeled as conv.opt.) are shown in first and third row. Figures in the second and fourth row marked with prop.opt depict the results obtained from probabilistic optimization.

using a regular desktop machine. ‡

Three-dimensional $\gamma$-pass rates according to Low et.al. (1998), utilizing a distance

‡ macOS Sierra, 2.7 GHz Intel Core i7, 16GB 2133 MHz RAM

to agreement of 2 mm and a dose difference criterion of 2 % were calculated and shown in Table 2. Results have to be interpreted with caution because random sampling is subject to uncertainty. Nevertheless, there is a good match between approximated analytical and sampling based quantities therefore justifying the approximations made in sections 2.3 and 2.4 to assess $\hat{\mathbb{E}}[\boldsymbol{\varepsilon}]$ and $\hat{\sigma}[\boldsymbol{\varepsilon}]$. The decrease of the $\gamma$-pass rates from $\hat{\mathbb{E}}[\boldsymbol{\varepsilon}]$ and $\hat{\sigma}[\boldsymbol{\varepsilon}]$ to $\hat{\mathbb{E}}[RBE \times d_p]$ and $\hat{\sigma}[RBE \times d_p]$ can be attributed to inaccuracies in the error propagation (see section 2.6). All $\gamma$-pass rates comparing approximated analytical and sampled quantities are above 94.95 %.

| | | conv.opt. | | prob.opt. | |
|---|---|---|---|---|---|
| case | resolution [mm] | $\mathbb{E}[\boldsymbol{\varepsilon}]$ | $\sigma[\boldsymbol{\varepsilon}]$ | $\mathbb{E}[\boldsymbol{\varepsilon}]$ | $\sigma[\boldsymbol{\varepsilon}]$ |
| intra-cranial | $1.1 \times 1.1 \times 3$ | 100 % | 99.88 % | 100 % | 99.82 % |
| paraspinal | $3 \times 3 \times 3$ | 99.71 % | 97.56 % | 99.98 % | 98.30 % |
| prostate | $3 \times 3 \times 3$ | 100 % | 99.41 % | 99.49 % | 98.70 % |
| | | $\mathbb{E}[RBE \times d_p]$ | $\sigma[RBE \times d_p]$ | $\mathbb{E}[RBE \times d_p]$ | $\sigma[RBE \times D]$ |
| intra-cranial | $1.1 \times 1.1 \times 3$ | 100 % | 98.82 % | 100 % | 99.44 % |
| paraspinal | $3 \times 3 \times 3$ | 99.99 % | 94.95 % | 99.15 % | 96.28 % |
| prostate | $3 \times 3 \times 3$ | 100 % | 98.76 % | 97.63 % | 97.56 % |

Table 2: Global $\gamma$-pass rates for the expectation value and standard deviation of the biological effect and RBE-weighted dose on basis of analytical calculations and random sampling (5000 samples). Three patient cases are under investigation considering one fraction. The abbreviation conv.opt indicates conventional optimization whereas prob.opt. denotes probabilistic optimization. A distance to agreement of 2 mm and a dose difference criteria of 2 % was used for the $\gamma$-analysis.

Figure 5 depicts the standard deviation volume histograms of all patient cases thereby explicitly comparing the results obtained via conventional optimization (no robustness considered) and probabilistic optimization (robustness consideration). The standard deviation histograms, which provide comprehensive information about the dose uncertainty within a specific volume of interest are in agreement with the single slice displays of the standard deviation in Figure 4.

## 4. Discussion

We demonstrated the feasibility of analytical computations of the expected value and variance of the biological effect and RBE-weighted dose in intensity-modulated carbon ion therapy considering setup and range uncertainties. The entire analytical pipeline for carbon ion therapy maintains compatibility with APM's core advantages allowing for (i) multi-dimensional linearly correlated random input variables , (ii) the definition of arbitrary correlation models, (iii) subsequent probabilistic optimization.
We decided to built APM upon the biological effect to avoid integrating Equation 1 with the square root dependence against Gaussian densities. Besides analytical solutions, we introduced analytical approximations which effectively reduce the number of operations (i) for the expected biological effect from $\mathcal{O}(V \times B^2)$ to $\mathcal{O}(V \times B)$ and (ii) for the variance of the biological effect from $\mathcal{O}(V \times B^4)$ to $\mathcal{O}(V \times B^2)$ both at marginal loss in accuracy. We want to point out that the observed discrepancies between APM computations and 5000 samples for $\hat{\mathbb{E}}[\boldsymbol{\varepsilon}]$ and $\hat{\sigma}[\boldsymbol{\varepsilon}]$ are not only related to the approximations within the APM formalism but also due to residual statistical

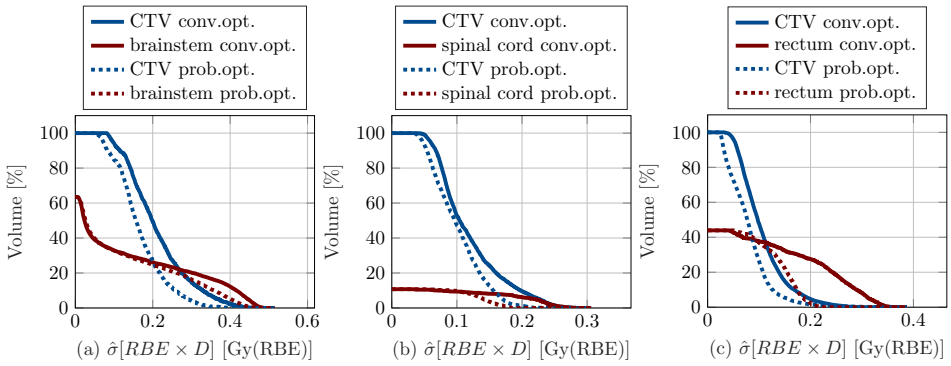


Figure 5: Standard deviation volume histograms of the RBE-weighted dose for the (5a) intra-cranial case assuming 1 fraction, (5b) the para-spinal case assuming 5 fraction, and (5c) the prostate case optimized for 30 fractions. Solid lines represent the results obtained from conventional optimization (conv.opt) and dashed lines are based on probabilistic APM optimization (prob.opt.).

uncertainty in the sampling based reference. Furthermore, we demonstrated on three patient cases that APM can effectively be used for uncertainty minimization through probabilistic optimization of the biological effect.

The calculation of the expected biological effect exhibits the same computational complexity as the nominal biological effect $\mathcal{O}(V \times B)$, assessing its variance using the proposed method requires $\mathcal{O}(V \times B^2)$ operations. Consequently, the most time critical treatment plan parameters are the pencil beam grid spacing and the number of pencil beam contributions to voxel $i$. Despite the fact that carbon ions exhibit ∼3 times less lateral scattering compared to protons, the number of dose deposition points is usually higher for carbon ions due to the fragmentation tail. For this reasons, APM calculation times for carbons ions are in general longer compared to protons. Our current prototype implementation in the interpreted programming language Matlab still requires comparably long computations (4-7h per patient case). To increase runtime, an implementation in our C++ based in-house treatment planning system built upon the MITK framework (Wolf et al. 2005) is part of ongoing work. In general, we expect a similar relative performance for carbon ions like for protons where we have already shown that APM enables effective uncertainty quantification and probabilistic treatment plan optimization for protons using a constant RBE with total runtimes of a view minutes using our C++ in-house treatment planning system on regular desktop machines (Wahl et al. 2017). In particular, it could be established that APM generally exhibits a better trade-off between speed and accuracy compared to sampling-based uncertainty quantification and minimization - especially in the context of fractionated radiation therapy (Wahl et al. 2017).

In contrast, to the work based on the same APM concept presented in (Bangert et al. 2013, Wahl et al. 2017), who modeled the impact of physical uncertainties on the physical dose, this work is about the impact of physical uncertainties on the biological effect considering a variable RBE and the correlation between physical and biological beam properties. A direct application of the physical dose based formalism presented by (Bangert et al. 2013, Wahl et al. 2017) to carbon ion treatment planning is not suited as it does not model the dependence of RBE on the particle spectra,

tissue type and dose level.

Although we observe a maximal discrepancy of 5.2 % comparing the approximated variance against sampled references for the 1D SOBP, we argue that these discrepancy are mitigated in a clinically three-dimensional treatment plan because of two reasons. (i) We usually do not see such steep dose gradients and (ii) lateral neighboring pencil beam will also have an influence and will consequently lower the variance.

The nonlinear propagation of moments of the biological effect to moments of the RBE-weighted dose is achieved via a Taylor expansion around $\mathbb{E}[\boldsymbol{\varepsilon}]$. Although the distribution over the biological effect is non-Gaussian and the RBE-weighted dose computation itself is nonlinear, the error propagation only slightly diminishes the accuracy of APM calculations against random sampling results (see Table 2). Calculating higher order moments $n > 2$ (skewness and kurtosis) of the biological effect would in principle permit a more precise shape description of the unknown probability distribution of the biological effect $\varepsilon_i$ in voxel $i$.

Throughout this work, the lateral dose was only modeled by a single Gaussian component which might not model the low-dose halo accurately enough. In general, our considerations also apply to double or triple Gaussian lateral beam models. Similar to the depth components, the lateral dose could then also be modelled with a superposition of Gaussians.

Setup and range uncertainties are modelled in this article by multivariate normal distributions. Whilst it is common practice to describe uncertainties in the context of radiotherapy with Gaussian probability densities, the APM framework also facilitates to model uniform distribution or any arbitrary probability density by a superposition of Gaussians. The latter illustrates again the core concept of APM, which is the approximation of not-integrable functions by a set of easily integrable functions - in this case Gaussians - to solve Equation 4 in closed-form.

We want to point out that we assumed a single biological system for treatment planning and did not assigned different photon LQ model radio-sensitives to individual structures. But we want to point out that it is in principle possible to use different $\frac{\alpha_x}{\beta_x}$ ratios for different tissues in our approach if desired by the planner. As all results presented in this manuscript refer to photon LQ model parameter $\alpha_x = 0.1\,\mathrm{Gy}^{-1}$ and $\beta_x = 0.05\,\mathrm{Gy}^{-2}$, we also evaluated and concluded that the mathematical deviations and approximations also hold for $\alpha_x = 0.5\,\mathrm{Gy}^{-1}$ and $\beta_x = 0.05\,\mathrm{Gy}^{-2}$.

The approach presented in this paper is generally applicable to biological treatment planning using other ion species such as protons or helium ions, provided that dose-averaged particle radio-sensitivity curves are available for various initial beam energies. APM does not depend on the underlying biophysical model; it allows for the incorporation of biological base data from other biophysical or phenomenological models.

The radio-sensitivity parameters of heavier ions are subjected to pronounced uncertainties, however, their variability has never been taken into account during optimization. This work may be the basis to account for uncertainties in the particle $\alpha_p$ and $\beta_p$ parameters of the LQ model. In particular, APM's capability to incorporate arbitrary correlation assumptions might be beneficial when modeling radio-sensitivity uncertainties (i) between $\alpha_p$ and $\beta_p$ parameters (ii) along penetrated tissues for individual pencil beams. This would allow to not only incorporate physical but also biological uncertainties into the treatment planning process of charged particles.

## 5. Conclusion

Using analytical probabilistic modeling, it is possible to calculate the expectation value and variance of RBE-weighted dose distributions in intensity-modulated scanned carbon ion therapy in closed-form considering setup and range errors including fractionation effects. Using low-rank approximations for the required tensor computations, it is possible to perform the nonlinear computations of the RBE-weighted dose at the same computational complexity like the linear computations of the physical dose at minimal loss of accuracy. We compare APM moment calculations for three patient cases against sampling-based references and observe global $\gamma$-pass rates [2 mm, 2 %] of >99.15 % for the expectation value and >94.95 % for the standard deviation of the RBE-weighted dose. All mathematical derivations for calculating statistical moments of the biological effects maintain compatibility with APM's special features of (i) enabling multi-dimensional linearly correlated random input variables (ii) modelling arbitrary correlations (iii) generalizing to probabilistic optimization.

## 6. Acknowledgements

We would like to thank the Probabilistic Numerics Group of the Max Planck Institute for Intelligent Systems in Tübingen for helpful discussion. Financial support from the German Research Foundation, Grant No. BA 2279/3-1 is gratefully acknowledged.

## 7. References

Albertini, F., Hug, E. B. & Lomax, A. J. (2011), 'Is it necessary to plan with safety margins for actively scanned proton therapy?', *Physics in Medicine and Biology* **56**(14), 4399–4413.

Anderson, T. V. & Mattson, C. A. (2012), 'Propagating Skewness and Kurtosis Through Engineering Models for Low-Cost, Meaningful, Nondeterministic Design', *Journal of Mechanical Design* **134**(10), 100911.

Baum, C., Alber, M., Birkner, M. & Nüsslin, F. (2004), 'Treatment simulation approaches for the estimation of the distributions of treatment quality parameters generated by geometrical uncertainties.', *Physics in medicine and biology* **49**(24), 5475–5488.

Bangert, M., Hennig, P. & Oelfke, U. (2013). Analytical probabilistic modeling for radiation therapy treatment planning, *Physics in Medicine and Biology* **58**(16): 5401–5419.

Baum, C., Alber, M., Birkner, M. & Nüsslin, F. (2004). Treatment simulation approaches for the estimation of the distributions of treatment quality parameters generated by geometrical uncertainties., *Physics in Medicine and Biology* **49**(24): 5475–5488.

Chen, W., Unkelbach, J., Trofimov, A., Madden, T., Kooy, H., Bortfeld, T. & Craft, D. (2012). Including robustness in multi-criteria optimization for intensity-modulated proton therapy, *Physics in Medicine and Biology* **57**: 591–608.

Elsässer, T., Weyrather, W. K., Friedrich, T., Durante, M., Iancu, G., Krämer, M., Kragl, G., Brons, S., Winter, M., Weber, K. J. & Scholz, M. (2010). Quantification of the relative biological effectiveness for ion beam radiotherapy: Direct experimental comparison of proton and carbon ion beams and a novel approach for treatment planning, *International Journal of Radiation Oncology Biology Physics* **78**: 1177–1183.

Fredriksson, A., Forsgren, A. & Hårdemark, B. (2011). Minimax optimization for handling range and setup uncertainties in proton therapy, *Medical Physics* **38**(3): 1672–1684.

Gottschalk, B., Koehler, A. M., Schneider, R. J., Sisterson, J. M. & Wagner, M. S. (1993). Multiple Coulomb scattering of 160 MeV protons, *Nuclear Inst. and Methods in Physics Research, B* **74**(4): 467–490.

Hong, L., Goitein, M., Bucciolini, M., Comiskey, R., Gottschalk, B., Rosenthal, S., Serago, C. & Urie, M. (1996). A pencil beam algorithm for proton dose calculations, *Physics in Medicine and Biology* **41**(8): 1305–1330.

O. Jäkel, M. Krämer, C. P. Karger, J. D. (2001), 'Treatment planning for heavy ion radiotherapy : clinical implementation and application',*Physics in Medicine and Biology* **46**(4), 1101–1116.

Kamp, F., Brüningk, S., Cabal, G., Mairani, a., Parodi, K. & Wilkens, J. J. (2014). Variance-based sensitivity analysis of biological uncertainties in carbon ion therapy, *Physica Medica* **30(5)**:583-587.

Kellerer, A. M. & Rossi, H. H. (1978). A Generalized Formulation of Dual Radiation Action, *Radiation Research* **75**(3): 471.

Krämer, M. & Scholz, M. (2006). Rapid calculation of biological effects in ion radiotherapy., *Physics in Medicine and Biology* **51**: 1959–1970.

Lehmann, E. L. & Casella, G. (1998). *Theory of Point Estimation (Springer Texts in Statistics)*, 2nd edn, Springer.

Liu, W., Frank, S. J., Li, X., Li, Y., Park, P. C., Dong, L., Ronald Zhu, X. & Mohan, R. (2013), 'Effectiveness of robust optimization in intensity-modulated proton therapy planning for head and neck cancers.', *Medical physics* **40**(5), 051711.

Liu, W., Zhang, X., Li, Y. & Mohan, R. (2012). Robust optimization of intensity modulated proton therapy., *Medical Physics* **39**(2): 1079–1091.

Lomax, A. J. (2008a). Intensity modulated proton therapy and its sensitivity to treatment uncertainties 1: the potential effects of calculational uncertainties., *Physics in Medicine and Biology* **53**(4): 1027–1042.

Lomax, A. J. (2008b). Intensity modulated proton therapy and its sensitivity to treatment uncertainties 2: the potential effects of inter-fraction and inter-field motions, *Physics in Medicine and Biology* **53**(4): 1043–1056.

Lomax, A. J. (2008*c*), Intensity Modulated Proton Therapy, T. Delaney & H. Kooy, 'Proton and Charged Particle Radiotherapy', Lippincott Williams & Wilkins.

Low, D. A., Harms, W. B., Mutic, S. & Purdy, J. A. (1998). A technique for the quantitative evaluation of dose distributions, *Medical Physics* **25**(5): 656.

Lowe, M., Albertini, F., Aitkenhead, A., Lomax, A. J. & MacKay, R. I. (2016), 'Incorporating the effect of fractionation in the evaluation of proton plan robustness to setup errors', *Physics in Medicine and Biology* **61**(1), 413–429.

Paganetti, H. (2012). Range uncertainties in proton therapy and the role of Monte Carlo simulations, *Physics in Medicine and Biology* **57**: R99–R117.

Park, P. C., Cheung, J., Zhu, X. R., Sahoo, N., Court, L. & Dong, L. (2012). Fast range-corrected proton dose approximation method using prior dose distribution, *Physics in Medicine and Biology* **57**(11): 3555–3569.

Parodi, K., Mairani, A., Brons, S., Hasch, B. G., Sommerer, F., Naumann, J., Jäkel, O., Haberer, T. & Debus, J. (2012). Monte Carlo simulations to support start-up and treatment planning of scanned proton and carbon ion therapy at a synchrotron-based facility, *Physics in Medicine and Biology* **57**(12): 3759–3784.

Perkó, Z., van der Voort, S. R., van de Water, S., Hartman, C. M. H., Hoogeman, M. & Lathouwers, D. (2016). Fast and accurate sensitivity analysis of IMPT treatment plans using Polynomial Chaos Expansion., *Physics in Medicine and Biology* **61**(12): 4646–64.

Pflugfelder, D., Wilkens, J. J. & Oelfke, U. (2008). Worst case optimization: a method to account for uncertainties in the optimization of intensity modulated proton therapy, *Physics in Medicine and Biology* **53**(53): 1689–1700.

Rose, C. & Smith, M. D. (2002). *mathStatica: Mathematical Statistics with Mathematica*, Physica-Verlag HD, Heidelberg, pp. 437–442.

Sakama, M., Kanematsu, N. & Inaniwa, T. (2016). A robustness analysis method with fast estimation of dose uncertainty distributions for carbon-ion therapy treatment planning, *Physics in Medicine and Biology* **61**(15): 5818–5836.

Schaffner, B., Pedroni, E. & Lomax, A. (1999), 'Dose calculation models for proton treatment planning using a dynamic beam delivery system: an attempt to include density heterogeneity effects in the analytical dose calculation.', *Physics in Medicine and Biology* **44**(1), 27–41.

Scholz, M. & Kraft, G. (1996). Track structure and the calculation of biological effects of heavy charged particles, *Advances in Space Research* **18**(1-2): 5–14.

Siddon, R. L. (1984). Fast calculation of the exact radiological path for a three-dimensional CT array., *Medical Physics* **12**(2): 252–255.

Siggel, M., Ziegenhein, P., Nill, S. & Oelfke, U. (2012). Boosting runtime-performance of photon pencil beam algorithms for radiotherapy treatment planning, *Physica Medica* **28**(4): 273–280.

Sobotta, B., Söhn, M. & Alber, M. (2012). Accelerated evaluation of the robustness of treatment plans against geometric uncertainties by Gaussian processes, *Physics in Medicine and Biology* **57**(23): 8023–8039.

Squires, G. L. (2001), *Practical Physics*, Cambridge University Press, Cambridge.

Steitz, J., Naumann, P., Ulrich, S., Haefner, M. F., Sterzing, F., Oelfke, U. & Bangert, M. (2016).

Worst case optimization for interfractional motion mitigation in carbon ion therapy of pancreatic cancer, *Radiation Oncology* **11**(1): 134.

Suit, H., DeLaney, T., Goldberg, S., Paganetti, H., Clasie, B., Gerweck, L., Niemierko, A., Hall, E., Flanz, J., Hallman, J. & Trofimov, A. (2010), 'Proton vs carbon ion beams in the definitive radiation treatment of cancer patients', *Radiotherapy and Oncology* **95**(February 2009), 3–22.

Unkelbach, J., Bortfeld, T., Martin, B. C. & Soukup, M. (2009). Reducing the sensitivity of IMPT treatment plans to setup errors and range uncertainties via probabilistic treatment planning., *Medical Physics* **36**(1): 149–163.

Unkelbach, J., Chan, T. C. Y. & Bortfeld, T. (2007). Accounting for range uncertainties in the optimization of intensity modulated proton therapy., *Physics in Medicine and Biology* **52**(10): 2755–73.

Unkelbach, J. & Oelfke, U. (2004). Inclusion of organ movements in IMRT treatment planning via inverse planning based on probability distributions., *Physics in Medicine and Biology* **49**(17): 4005–4029.

Van Herk, M. (2004). Errors and Margins in Radiotherapy, *Seminars in Radiation Oncology* **14**(1): 52–64.

Wahl N., Hennig P., Wieser HP., Bangert M. (2017). Efficency of analytical and sampling-based uncertainty propagation in intensity-modulated proton therapy, *Physics in Medicine and Biology* **62**(14): 5790–5807.

Wieser, H.-P., Cisternas, E., Wahl, N., Ulrich, S., Stadler, A., Mescher, H., Müller, L.-R., Klinge, T., Gabrys, H., Burigo, L., Mairani, A., Ecker, S., Ackermann, B., Ellerbrock, M., Parodi, K., Jäkel, O. & Bangert, M. (2017). Development of the open-source dose calculation and optimization toolkit matRad, *Medical Physics* **44**(6): 2556–2568.

Wilkens, J. J. & Oelfke, U. (2006). Fast multifield optimization of the biological effect in ion therapy., *Physics in Medicine and Biology* **51**: 3127–3140.

Wolf, I., Vetter, M., Wegner, I., Böttger, T., Nolden, M., Schöbinger, M., Hastenteufel, M., Kunert, T. & Meinzer, H.-P. (2005). The Medical Imaging Interaction Toolkit, *Medical Image Analysis* **9**(6): 594–604.

Zaider, M. & Rossi, H. H. (1980). The Synergistic Effects of Different Radiations, *Source: Radiation Research* **83**(3): 732–739.

## Appendix A. Analytical Probabilistic Modelling Notation

| Notation | Meaning | Description | Complexity |
|---|---|---|---|
| L | L | lateral dose in x, y | $\mathcal{O}(V \times B)$ |
| $\mathcal{L}$ | $\mathbb{E}[L]$ | 1st central moment of lateral dose | $\mathcal{O}(V \times B)$ |
| $\Upsilon$ | $\mathbb{E}[L^2]$ | 2nd central moment of lateral dose | $\mathcal{O}(V^2 \times B^2)$ |
| $Z$ | Z | depth dose in z | $\mathcal{O}(V \times B)$ |
| $\mathcal{Z}$ | $\mathbb{E}[Z]$ | 1st central moment of depth dose | $\mathcal{O}(V \times B)$ |
| $\Xi$ | $\mathbb{E}[Z^2]$ | 2nd central moment of depth dose | $\mathcal{O}(V^2 \times B^2)$ |
| D | $L^x L^y Z$ | dose influence matrix | $\mathcal{O}(V \times B)$ |
| $\mathcal{D}$ | $\mathbb{E}[D] = \mathcal{L}^x \mathcal{L}^y \mathcal{Z}$ | expected dose influence matrix | $\mathcal{O}(V \times B)$ |
| $\mathfrak{D}$ | $\mathbb{E}[D^2] = \Upsilon^x \Upsilon^y \Xi$ | 2nd central moment of dose influence matrix | $\mathcal{O}(V^2 \times B^2)$ |
| $\mathfrak{V}$ | $\Upsilon^x \Upsilon^y \Xi - \mathcal{D}^2$ | covariance influence tensor | $\mathcal{O}(V^2 \times B^2)$ |
| $Z^\alpha$ | $Z^\alpha$ | depth component $\alpha \circ d$ in z | $\mathcal{O}(V \times B)$ |
| $\mathcal{Z}^\alpha$ | $\mathbb{E}[Z^\alpha]$ | 1st central moment of depth $\alpha \circ d$ | $\mathcal{O}(V \times B)$ |
| $\Xi^\alpha$ | $\mathbb{E}[Z^{\alpha\,2}]$ | 2nd central moment of depth $\alpha \circ d$ | $\mathcal{O}(V^2 \times B^2)$ |
| $Z^{\sqrt{\beta}}$ | $Z^{\sqrt{\beta}}$ | depth component $\sqrt{\beta} \circ d$ | $\mathcal{O}(V \times B)$ |
| $\mathcal{Z}^{\sqrt{\beta}}$ | $\mathbb{E}[Z^{\sqrt{\beta}}]$ | 1st central moment of depth $\sqrt{\beta} \circ d$ | $\mathcal{O}(V \times B)$ |
| $\Xi^{\sqrt{\beta}}$ | $\mathbb{E}[Z^{\sqrt{\beta}\,2}]$ | 2nd central moment of depth $\sqrt{\beta} \circ d$ | $\mathcal{O}(V^2 \times B^2)$ |
| $A$ | $L^x L^y Z^\alpha$ | influence matrix of the linear term | $\mathcal{O}(V \times B)$ |
| $\mathcal{A}$ | $\mathbb{E}[A] = \mathcal{L}^x \mathcal{L}^y \mathcal{Z}^\alpha$ | expected linear term of bio. effect | $\mathcal{O}(V \times B)$ |
| $\Psi$ | $\mathbb{E}[A^2] = \Upsilon^x \Upsilon^y \Xi^\alpha$ | 2nd central moment of linear term of bio. effect | $\mathcal{O}(V^2 \times B^2)$ |
| $B$ | $L^x L^y Z^{\sqrt{\beta}}$ | influence matrix of the squared term | $\mathcal{O}(V \times B)$ |
| $\mathcal{B}$ | $\mathbb{E}[B] = \mathcal{L}^x \mathcal{L}^y \mathcal{Z}^{\sqrt{\beta}}$ | expected squared term of bio. effect | $\mathcal{O}(V \times B)$ |
| $\Phi$ | $\mathbb{E}[B^2] = \Upsilon^x \Upsilon^y \Xi^{\sqrt{\beta}}$ | 2nd central moment of squared term of bio. effect | $\mathcal{O}(V^2 \times B^2)$ |
| $\boldsymbol{\varepsilon}$ | $A\boldsymbol{w} + (B\boldsymbol{w})^2$ | biological effect | $\mathcal{O}(V \times B)$ |
| $\mathbb{E}[\boldsymbol{\varepsilon}]$ | $\mathcal{A}\boldsymbol{w} + \boldsymbol{w}^T \Phi \boldsymbol{w}$ | expected bio. effect | $\mathcal{O}(V \times B^2)$ |
| $\hat{\mathbb{E}}[\boldsymbol{\varepsilon}]$ | $\mathcal{A}\boldsymbol{w} + (\mathcal{B}\boldsymbol{w})^2$ | approx. expected bio. effect | $\mathcal{O}(V \times B)$ |
| $\mathfrak{D}^\varepsilon$ | - | 2nd central moment of bio. effect | $\mathcal{O}(V^2 \times B^4)$ |
| $\hat{\mathfrak{D}}^\varepsilon$ | - | approx. 2nd central moment of bio. effect | $\mathcal{O}(V^2 \times B^2)$ |
| $\hat{\mathfrak{V}}^\varepsilon$ | $\tilde{\mathfrak{D}}^\varepsilon - \hat{\mathbb{E}}[\boldsymbol{\varepsilon}]^2$ | approx. covariance influence tensor of bio. effect | $\mathcal{O}(V^2 \times B^2)$ |

Table A1: Notation used to describe APM for biological treatment planning

## Appendix B. Calculation of expected biological effect

Let $i, l$ be voxel indices and $j, m$ be pencil beam indices, $B$ be the number of pencil beams, then the full analytical calculation of the expectation value of the biological effect in voxel $i$ considering setup and range errors is given by:

$$\begin{aligned}
\mathbb{E}[\varepsilon_i] &= \int d\boldsymbol{\Delta}^x d\boldsymbol{\Delta}^y d\boldsymbol{\Delta}^z \, p(\boldsymbol{\Delta}^x) p(\boldsymbol{\Delta}^y) p(\boldsymbol{\Delta}^z) \varepsilon_i(\boldsymbol{\Delta}^x, \boldsymbol{\Delta}^y, \boldsymbol{\Delta}^z) \\
&= \int d\boldsymbol{\Delta}^x d\boldsymbol{\Delta}^y d\boldsymbol{\Delta}^z \, p(\boldsymbol{\Delta}^x) p(\boldsymbol{\Delta}^y) p(\boldsymbol{\Delta}^z) \left[ \sum_j^B w_j L_{ij}^x L_{ij}^y Z_{ij}^\alpha + \left( \sum_j^B w_j L_{ij}^x L_{ij}^y Z_{ij}^{\sqrt{\beta}} \right)^2 \right] \\
&= \sum_j^B w_j \left\{ \int d\boldsymbol{\Delta}^x p(\boldsymbol{\Delta}^x) L_{ij}^x \right\} \left\{ \int d\boldsymbol{\Delta}^y p(\boldsymbol{\Delta}^y) L_{ij}^y \right\} \left\{ \int d\boldsymbol{\Delta}^z p(\boldsymbol{\Delta}^z) Z_{ij}^\alpha \right\} \\
&\quad + \sum_{jm}^B w_j w_m \left\{ \int d\boldsymbol{\Delta}^x p(\boldsymbol{\Delta}^x) L_{ij}^x L_{im}^x \right\} \left\{ \int d\boldsymbol{\Delta}^y p(\boldsymbol{\Delta}^y) L_{ij}^y L_{im}^y \right\} \\
&\quad \left\{ \int d\boldsymbol{\Delta}^z p(\boldsymbol{\Delta}^z) Z_{ij}^{\sqrt{\beta}} Z_{im}^{\sqrt{\beta}} \right\} \\
&= \sum_j^B w_j \mathcal{L}_{ij}^x \mathcal{L}_{ij}^y \mathcal{Z}_{ij}^\alpha + \sum_{jm}^B w_j w_m \Upsilon_{ijim}^x \Upsilon_{ijim}^y \Xi_{ijim}^{\sqrt{\beta}}
\end{aligned} \tag{B.1}$$

According to (Bangert et al. 2013) Equation 13, the lateral components $\mathcal{L}_{ij}^{x/y}$ are given by

$$\mathcal{L}_{ij}^{x/y} = \frac{1}{\sqrt{2\pi(\lambda_{ij}^2 + \Sigma_{jj}^{x/y})}} e^{\frac{\left(x_{ij}/y_{ij} - \mu_j^{x/y}\right)^2}{2\left(\lambda_{ij}^2 + \Sigma_{jj}^{x/y}\right)}} \tag{B.2}$$

where $\lambda_{ij}^2$ denotes the variance of the lateral Gaussian beam profile at the respective radiological depth $z_{ij}$, $\Sigma_{jj}^{x/y}$ denotes the variance of pencil beam $j$ determining the setup error in $x/y$-dimension, $x_{ij}/y_{ij}$ depicts the lateral distance to the central ray. In analogy, the expected value $\mathcal{Z}_{ij}^\alpha$ of the alpha-dose $\boldsymbol{\alpha^c} \circ \boldsymbol{d}$ depth component considering $k = 1...13$ fitted Gaussian components with mean $\mu_{jk}^\alpha$, variance ${\delta_{jk}^\alpha}^2$ and weight $\omega_{jk}^\alpha$ is given by

$$\mathcal{Z}_{ij}^\alpha = \sum_{k=1}^{13} \frac{\omega_{jk}^\alpha}{\sqrt{2\pi({\delta_{jk}^\alpha}^2 + \Sigma_{jj}^z)}} e^{\frac{\left(z_{ij} - \mu_{jk}^\alpha\right)^2}{2\left({\delta_{jk}^\alpha}^2 + \Sigma_{jj}^z\right)}} \tag{B.3}$$

while $\Sigma_{jj}^z$ denotes the variance of the range error of pencil beam $j$. Equation B.3 is in close analogy to Equation 16 in (Bangert et al. 2013).

The remaining three components $\Upsilon_{ijlm}^x$, $\Upsilon_{ijlm}^y$ and $\Xi_{ijlm}^{\sqrt{\beta}}$ represent two-dimensional normal distributions and additionally require the calculation of covariance between pencil beams to assess the expectation value of the biological effect. With the two dimensional vectors $\boldsymbol{x}_{ijlm}$ and $\boldsymbol{\mu}_{jm}^x$ and the two dimensional matrices

$\Lambda_{ijlm}$, $\Sigma^x_{jm}$

$$\boldsymbol{x}_{ijlm} = \begin{pmatrix} x_{ij} \\ x_{lm} \end{pmatrix}, \quad \boldsymbol{\mu}^x_{jm} = \begin{pmatrix} \mu_j \\ \mu_m \end{pmatrix}$$
$$\Lambda_{ijlm} = \begin{pmatrix} \lambda^2_{ij} & 0 \\ 0 & \lambda^2_{lm} \end{pmatrix}, \quad \Sigma^x_{jm} = \begin{pmatrix} \Sigma^x_{jj} & \Sigma^x_{jm} \\ \Sigma^x_{mj} & \Sigma^x_{mm} \end{pmatrix} \tag{B.4}$$

the second raw moment of the lateral dose component in x-dimension $\Upsilon^x_{ijlm}$ is given by

$$\Upsilon^x_{ijlm} = \frac{1}{2\pi\sqrt{|\Lambda_{ijlm} + \Sigma^x_{jm}|}} e^{-\frac{1}{2}(\boldsymbol{x}_{ijlm} - \boldsymbol{\mu}^x_{jm})^T (\Lambda_{ijlm} + \Sigma^x_{jm})^{-1} (\boldsymbol{x}_{ijlm} - \boldsymbol{\mu}^x_{jm})} \tag{B.5}$$

Similar deviations can be found in (Bangert et al. 2013) in Equation 14. Finally, the second raw moment $\Xi^{\sqrt{\beta}}_{ijlm}$ of the $\sqrt{\boldsymbol{\beta}} \circ \boldsymbol{d}$ component can be calculated by defining:

$$\boldsymbol{z}_{ijlm} = \begin{pmatrix} z_{ij} \\ z_{lm} \end{pmatrix}, \quad \boldsymbol{\mu}^z_{jumv} = \begin{pmatrix} \mu^\beta_{ju} \\ \mu^\beta_{mv} \end{pmatrix}$$
$$\Theta^\beta_{jumv} = \begin{pmatrix} {\delta^\beta_{ju}}^2 & 0 \\ 0 & {\delta^\beta_{mv}}^2 \end{pmatrix}, \quad \Sigma^z_{jm} = \begin{pmatrix} \Sigma^z_{jj} & \Sigma^z_{jm} \\ \Sigma^z_{mj} & \Sigma^z_{mm} \end{pmatrix} \tag{B.6}$$

Following the deviation made in Equation 18 (Bangert et al. 2013) and defining $u$ and $v$ be indices of individual Gaussian components, then $\Xi^{\sqrt{\beta}}_{ijlm}$ results in:

$$\Xi^{\sqrt{\beta}}_{ijlm} = \sum_{uv=1}^{13} \frac{\omega^\beta_{ju}\omega^\beta_{mv}}{2\pi\sqrt{|\Theta^\beta_{jumv} + \Sigma^z_{jm}|}} e^{-\frac{1}{2}(\boldsymbol{z}_{ijlm} - \boldsymbol{\mu}^z_{jumv})^T (\Theta^\beta_{jumv} + \Sigma^z_{jm})^{-1} (\boldsymbol{z}_{ijlm} - \boldsymbol{\mu}^z_{jumv})} \tag{B.7}$$

## Appendix C. Calculation of variance of the biological effect

Let $i, l$ be voxel indices and $j, m, o, q$ be pencil beam indices, $B$ be the total number of pencil beams then the full analytical calculation of the covariance of the biological effect requires mixed terms $\mathbb{E}[\varepsilon_i \varepsilon_l]$, which can be calculated as follows:

$$\begin{aligned}
\mathbb{E}[\varepsilon_i \varepsilon_l] &= \int d\boldsymbol{\Delta}^x d\boldsymbol{\Delta}^y d\boldsymbol{\Delta}^z p(\boldsymbol{\Delta}^x) p(\boldsymbol{\Delta}^y) p(\boldsymbol{\Delta}^z) p(\boldsymbol{\Delta}^z) \epsilon_i(\boldsymbol{\Delta}^x, \boldsymbol{\Delta}^y, \boldsymbol{\Delta}^z) \epsilon_l(\boldsymbol{\Delta}^x, \boldsymbol{\Delta}^y, \boldsymbol{\Delta}^z) \\
&= \int d\boldsymbol{\Delta}^x d\boldsymbol{\Delta}^y d\boldsymbol{\Delta}^z p(\boldsymbol{\Delta}^x) p(\boldsymbol{\Delta}^y) p(\boldsymbol{\Delta}^z) p(\boldsymbol{\Delta}^z) \\
&\quad \left\{ \sum_j^B w_j L^x_{ij} L^y_{ij} Z^\alpha_{ij} + \left( \sum_j^B w_j L^x_{ij} L^y_{ij} Z^{\sqrt{\beta}}_{ij} \right)^2 \right\} \\
&\quad \left\{ \sum_m^B w_m L^x_{lm} L^y_{lm} Z^\alpha_{lm} + \left( \sum_m^B w_m L^x_{lm} L^y_{lm} Z^{\sqrt{\beta}}_{lm} \right)^2 \right\}
\end{aligned} \tag{C.1}$$

$$
\begin{aligned}
&= \sum_{jm}^{B} w_j w_m \left\{ \int d\boldsymbol{\Delta}^x p(\boldsymbol{\Delta}^x) L_{ij}^x L_{lm}^x \right\} \left\{ \int d\boldsymbol{\Delta}^y p(\boldsymbol{\Delta}^y) L_{ij}^x L_{lm}^x \right\} \left\{ \int d\boldsymbol{\Delta}^x p(\boldsymbol{\Delta}^x) Z_{ij}^{\alpha} Z_{lm}^{\alpha} \right\} + \\
&\sum_{jmq}^{B} w_j w_m w_q \left\{ \int d\boldsymbol{\Delta}^x p(\boldsymbol{\Delta}^x) L_{ij}^x L_{lm}^x L_{lq}^x \right\} \left\{ \int d\boldsymbol{\Delta}^y p(\boldsymbol{\Delta}^y) L_{ij}^y L_{lm}^y L_{lq}^y \right\} \left\{ \int d\boldsymbol{\Delta}^z p(\boldsymbol{\Delta}^z) Z_{ij}^{\alpha} Z_{lm}^{\sqrt{\beta}} Z_{lq}^{\sqrt{\beta}} \right\} + \\
&\sum_{jmo}^{B} w_j w_m w_o \left\{ \int d\boldsymbol{\Delta}^x p(\boldsymbol{\Delta}^x) L_{ij}^x L_{lm}^x L_{io}^x \right\} \left\{ \int d\boldsymbol{\Delta}^y p(\boldsymbol{\Delta}^y) L_{ij}^y L_{lm}^y L_{io}^y \right\} \left\{ \int d\boldsymbol{\Delta}^z p(\boldsymbol{\Delta}^z) Z_{ij}^{\alpha} Z_{lm}^{\sqrt{\beta}} Z_{io}^{\sqrt{\beta}} \right\} + \\
&\sum_{jmoq}^{B} w_j w_m w_o w_q \left\{ \int d\boldsymbol{\Delta}^x p(\boldsymbol{\Delta}^x) L_{ij}^x L_{io}^x L_{lm}^x L_{lq}^x \right\} \left\{ \int d\boldsymbol{\Delta}^y p(\boldsymbol{\Delta}^y) L_{ij}^y L_{io}^y L_{lm}^y L_{lq}^y \right\} \\
&\left\{ \int d\boldsymbol{\Delta}^z p(\boldsymbol{\Delta}^z) Z_{ij}^{\sqrt{\beta}} Z_{io}^{\sqrt{\beta}} Z_{lm}^{\sqrt{\beta}} Z_{lq}^{\sqrt{\beta}} \right\}
\end{aligned}
\tag{C.2}
$$

$$
\begin{aligned}
\mathbb{E}[\varepsilon_i \varepsilon_l] &= \sum_{jm}^{B} w_j w_m \Upsilon_{ijlm}^x \Upsilon_{ijlm}^y \Xi_{ijlm}^{\alpha} + 2 \sum_{jmo}^{B} w_j w_m w_o \Upsilon_{ijlmio}^x \Upsilon_{ijlmio}^y \Xi_{ijlmio}^{\alpha 2\sqrt{\beta}} + \\
&\sum_{jmoq}^{B} w_j w_m w_o w_q \Upsilon_{ijiolmlq}^x \Upsilon_{ijiolmlq}^y \Xi_{ijiolmlq}^{\sqrt{\beta}}
\end{aligned}
\tag{C.3}
$$

Considering only the variance, which is stored in the diagonal of the covariance matrix, we can set $i = l$ and can then obtain:

$$
\begin{aligned}
\mathbb{E}[\varepsilon_i \varepsilon_i] &= \sum_{jm}^{B} w_j w_m \Upsilon_{ijm}^x \Upsilon_{ijm}^y \Xi_{ijm}^{\alpha} + 2 \sum_{jmo}^{B} w_j w_m w_o \Upsilon_{ijmo}^x \Upsilon_{ijmo}^y \Xi_{ijmo}^{\alpha 2\sqrt{\beta}} + \\
&\sum_{jmoq}^{B} w_j w_m w_o w_q \Upsilon_{ijmoq}^x \Upsilon_{ijmoq}^y \Xi_{ijmoq}^{\sqrt{\beta}}
\end{aligned}
\tag{C.4}
$$

Exemplary, the calculation of $\Xi_{ijlmpq}^{\alpha 2\sqrt{\beta}}$ is shown below (calculations for $\Upsilon_{ijlmpq}^{x/y}$ can be done in a similar fashion). Given $i, l, p$ depict voxel indices, $j, m, q$ spot indices and $u$,$v$,$w$ individual Gaussian components, we can define

$$
\begin{aligned}
&\boldsymbol{z}_{ijlmpq} = \begin{pmatrix} z_{ij} \\ z_{lm} \\ z_{pq} \end{pmatrix}, \quad \boldsymbol{\mu}_{jumvqw}^z = \begin{pmatrix} \mu_{ju}^{\alpha} \\ \mu_{mv}^{\beta} \\ \mu_{qw}^{\beta} \end{pmatrix} \quad \boldsymbol{\Delta}_{jmq}^z = \begin{pmatrix} \Delta_j^z \\ \Delta_m^z \\ \Delta_q^z \end{pmatrix} \\
&\Theta_{jumvqw} = \begin{pmatrix} {\delta_{ju}^{\alpha}}^2 & 0 & 0 \\ 0 & {\delta_{mv}^{\beta}}^2 & 0 \\ 0 & 0 & {\delta_{qw}^{\beta}}^2 \end{pmatrix}, \quad \Sigma_{jmq}^z = \begin{pmatrix} \Sigma_{jj}^z & \Sigma_{mj}^z & \Sigma_{qj}^z \\ \Sigma_{jm}^z & \Sigma_{mm}^z & \Sigma_{qm}^z \\ \Sigma_{jq}^z & \Sigma_{mq}^z & \Sigma_{qq}^z \end{pmatrix}
\end{aligned}
\tag{C.5}
$$

to solve

$$
\begin{aligned}
\Xi^{\alpha 2\sqrt{\beta}}_{ijlmpq} &= \int d\boldsymbol{\Delta}^z p(\boldsymbol{\Delta}^z) Z^{\alpha}_{ij} Z^{\sqrt{\beta}}_{lm} Z^{\sqrt{\beta}}_{pq} \\
&= \int d\boldsymbol{\Delta}^z p(\boldsymbol{\Delta}^z) \sum_{uvw=1}^{13} \frac{\omega^{\alpha}_{ju}}{\sqrt{2\pi {\delta^{\alpha}_{ju}}^2}} e^{\frac{(z_{ij}-\mu^{\alpha}_{ju})^2}{2{\delta^{\alpha}_{ju}}^2}} \frac{\omega^{\beta}_{mv}}{\sqrt{2\pi {\delta^{\beta}_{mv}}^2}} e^{\frac{(z_{lm}-\mu^{\beta}_{mv})^2}{2{\delta^{\beta}_{mv}}^2}} \frac{\omega^{\beta}_{qw}}{\sqrt{2\pi {\delta^{\beta}_{qw}}^2}} e^{\frac{(z_{pq}-\mu^{\beta}_{qw})^2}{2{\delta^{\beta}_{qw}}^2}} \\
&= \int d\boldsymbol{\Delta}^z p(\boldsymbol{\Delta}^z) \sum_{uvw=1}^{13} \frac{\omega^{\alpha}_{ju}\omega^{\beta}_{mv}\omega^{\beta}_{qw}}{(2\pi)^{\frac{3}{2}}\sqrt{|\Theta_{jumvqw}|}} e^{-\frac{1}{2}(\boldsymbol{z}_{ijlmpq}-\boldsymbol{\mu}^z_{jumvqw})^T(\Theta_{jumvqw})^{-1}(\boldsymbol{z}_{ijlmpq}-\boldsymbol{\mu}^z_{jumvqw})} \\
&= \sum_{uvw=1}^{13} \omega^{\alpha}_{ju}\omega^{\beta}_{mv}\omega^{\beta}_{qw} \int d\boldsymbol{\Delta}^z_{jmq} \frac{1}{(2\pi)^{\frac{3}{2}}\sqrt{|\Sigma^z_{jmq}|}} \\
&\quad \frac{1}{(2\pi)^{\frac{3}{2}}\sqrt{|\Theta_{jumvqw}|}} e^{-\frac{1}{2}(\boldsymbol{z}_{ijlmpq}-\boldsymbol{\mu}^z_{jumvqw})^T(\Theta_{jumvqw})^{-1}(\boldsymbol{z}_{ijlmpq}-\boldsymbol{\mu}^z_{jumvqw})} \\
&= \sum_{uvw=1}^{13} \frac{\omega^{\alpha}_{ju}\omega^{\beta}_{mv}\omega^{\beta}_{qw}}{(2\pi)^{\frac{3}{2}}\sqrt{|\Theta_{jumvqw}+\Sigma^z_{jmq}|}} e^{-\frac{1}{2}(\boldsymbol{z}_{ijlmpq}-\boldsymbol{\mu}^z_{jumvqw})^T(\Theta_{jumvqw}+\Sigma^z_{jmq})^{-1}(\boldsymbol{z}_{ijlmpq}-\boldsymbol{\mu}^z_{jumvqw})}
\end{aligned}
\tag{C.6}
$$

Calculations for $\Upsilon^{x/y}_{ijlmpqno}$ and $\Xi^{\sqrt{\beta}}_{ijlmpqno}$ are not explicitly stated here as their deviations are in close analogy to $\Xi^{\alpha 2\sqrt{\beta}}_{ijlmpq}$. Instead of integrating over a three-dimensional Gaussian the integration is thereby done over four-dimensional Gaussian distributions.